From Cells to Innovation: Leveraging Toxicological Tools for Safer Treatments

Expert Insights

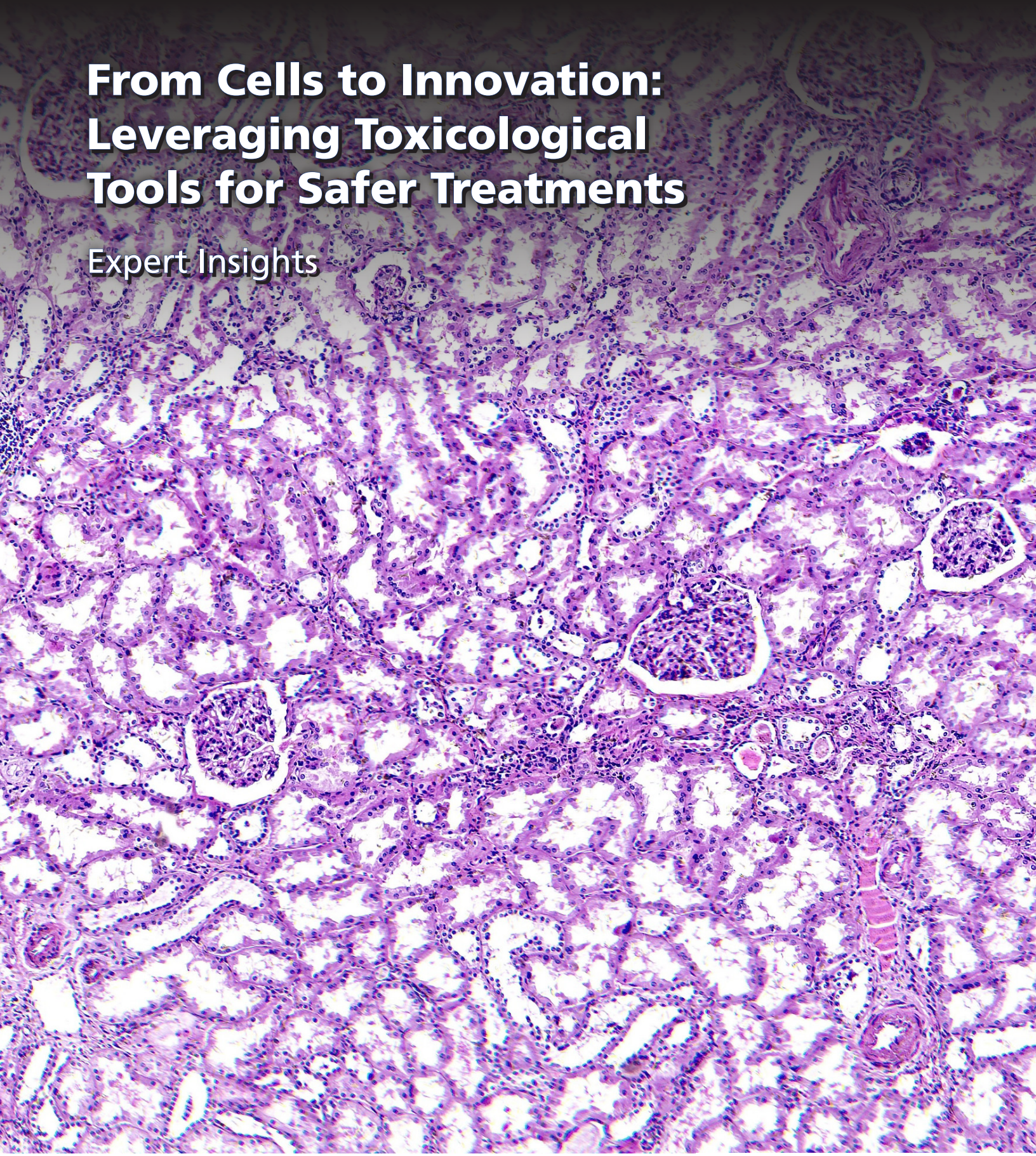

Sponsored by:

ATCC®

CURRENT PROTOCOLS
A Wiley Brand

WILEY

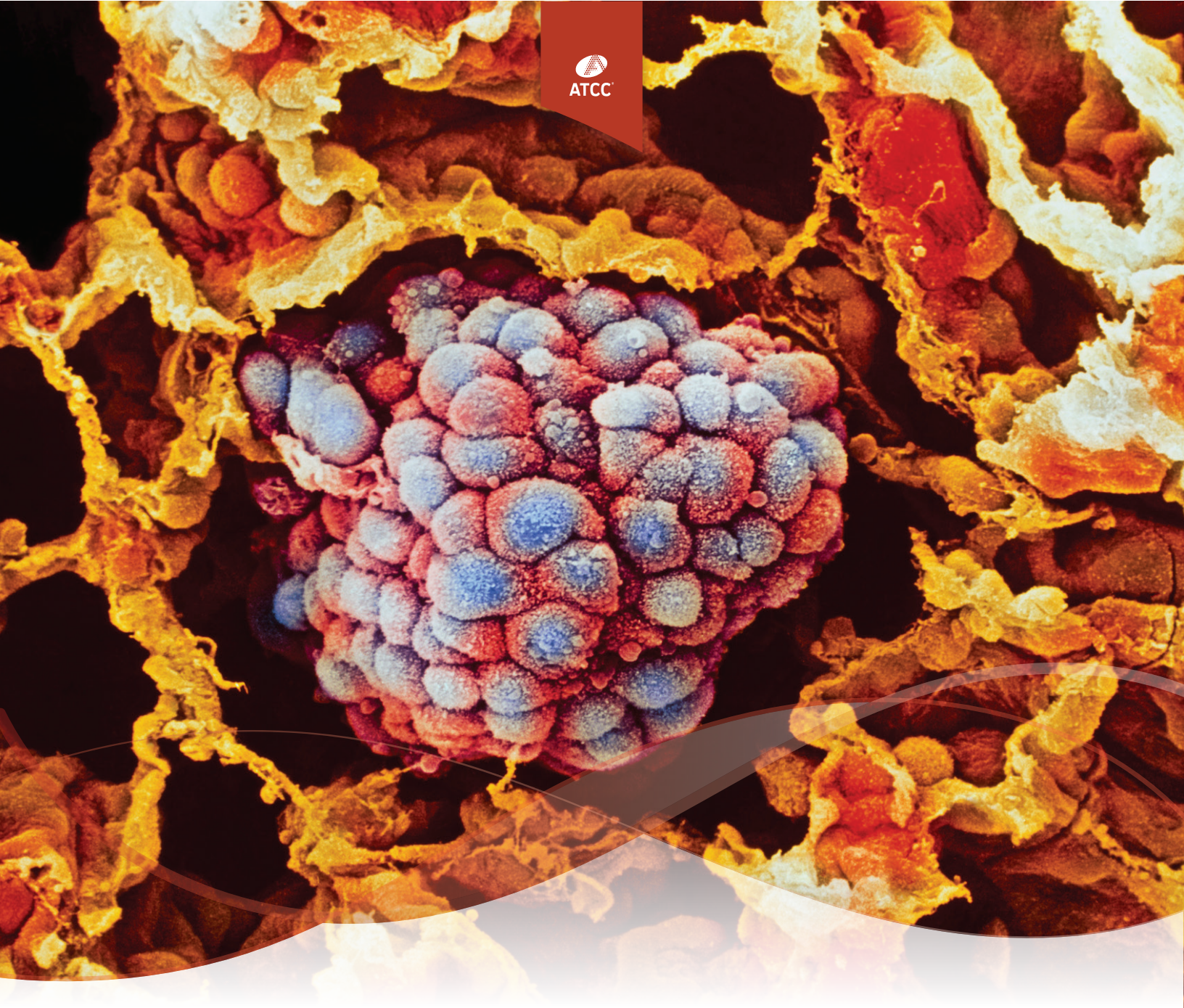

Where are you in your Toxicology Workflow

ATCC offers the cells, media, and reagents needed to explore each step of the in vitro preclinical testing process—from modeling, screening, and characterization to exploratory toxicology, pharmacokinetics, and metabolism. Count on ATCC models to help you identify adverse effects of your drug candidates and compounds for predictive, large-scale experiments to get your results and rule out toxicities faster.

- Continuous Cancer cell lines
- hTERT-immortalized primary cells
- Immune Cell lines
- Primary Cells
- Induced Pluripotent Stem Cells
- Neural Progenitor cells

Explore our Toxicology Portfolio
www.atcc.org/tox

ATCC® | Credible leads to Incredible®

Contents

Imprint

111 River Street,
Hoboken, NJ 07030-5774
USA
Contact: Customer Service

Editor:
Róisín Murtagh

Senior Account Manager:
Joseph Tomaszewski

ATCC
https://www.atcc.org/

Introduction

In toxicology, ensuring the safety of individuals and the environment requires an accurate assessment of the potential harmful effects caused by substances. This necessitates the utilization of authenticated model organisms and standardized testing methodologies for investigating renal, neural, airway, and skin toxicity. Advanced cell models enable researchers to perform a wide range of toxicological applications such as high-content screening, 3D culture, and permeability assays. By leveraging these resources, researchers can effectively identify and analyze responses to environmental insults as well as screen potential pharmaceutical compounds. This contributes to a better understanding of the adverse effects of various substances and aids in the development of safer and more effective treatments.

The tools and techniques toxicologists use to investigate substances may include *in vitro* studies using cell cultures and molecular techniques or *in vivo* studies using animal models. In recent years, there has been a growing emphasis on the development and utilization of alternative methods, such as *in silico* models and organ-on-a-chip technologies, which aim to reduce the reliance on animal testing while maintaining the accuracy and reliability of toxicological assessments.

The findings and insights from toxicology studies are crucial for various fields and industries. For example, in the pharmaceutical industry, toxicology plays a vital role in drug development by identifying potential toxic effects and establishing safe dosage ranges. In environmental toxicology, the discipline helps assess the impact of pollutants and contaminants on ecosystems and human health. Additionally, toxicology plays a pivotal role in chemical safety evaluation, occupational health, and regulatory decision-making processes. The field of toxicology continues to evolve as new substances and technologies emerge. This includes the study of the toxic effects of emerging contaminants, such as microplastics and nanomaterials, and the exploration of the toxicological implications of new technologies like gene editing and artificial intelligence. Furthermore, an understanding of nephrotoxicity is becoming increasingly important as the field of toxicology expands to encompass the study of emerging contaminants and technologies. Nephrotoxicity is a significant concern in toxicology as the kidneys play a crucial role in filtering waste and maintaining fluid and electrolyte balance in the body. Exposure to certain substances can cause damage to the renal cells and impair their function, leading to kidney dysfunction and potentially severe health complications.

This Expert Insights begins with an investigation [1] on the use of an improved *in vitro* human proximal tubule tissue model for studying nephrotoxicity. The hTERT[1]-immortalized model involves co-culturing renal proximal tubule epithelial cells (RPTECs) with renal fibroblasts and endothelial cells on a layered extracellular matrix. The co-cultured RPTECs showed more elongated branches and expressed multiple biomarkers in a more polarized distribution compared to RPTECs in monocultures. This result is important because it suggests that the co-culture model of RPTECs may have greater physiological relevance compared to monocultures and that the presence of other cell types in the co-culture system may enhance the functional characteristics of the renal proximal tubule cells. This could potentially make the co-culture model more suitable for studying nephrotoxicity and other renal-related phenomena, as it better mimics the complex cellular interactions and tissue organization found in the kidneys.

Next is a study [2] on the effect of euxanthone on airway epithelial cells (AECs) in the context of asthma progression. Euxanthone, a naturally occurring compound known for its cytotoxic activity against cancer and neurological disorders, was found to modulate lipopolysaccharide (LPS)-induced responses in AECs. LPS exposure of the *in vitro* cell models BAES-2B and 16HBE led to reduced cell viability, increased apoptosis and lactate dehydrogenase release, and elevated secretion of inflammatory cytokines and MUC5AC glycoprotein. However, simultaneous treatment with euxanthone inhibited the LPS-induced injury, inflammation, and mucus hypersecretion in the AECs. The study also suggested that this effect was mediated through the modulation of the TLR4/MyD88 pathway.

Through the methods and applications presented in this Expert Insights, we hope to educate scientists on new technologies and methodologies for toxicology research. To gain a deeper understanding of available options for improving your research, we encourage you to visit ATCC. Additionally, we recommend checking out this captivating webinar on primary airway cells in 3D models.

Róisín Murtagh
Editor at Wiley Analytical Science

[1] Human telomerase reverse transcriptase

References

[1] Wang, X. et al. (2020). Developing a self-organized tubulogenesis model of human renal proximal tubular epithelial cells in vitro. *Journal of Biomedical Materials Research - Part A.* DOI: 10.1002/jbm.a.36858.

[2] Shen, W. et al. (2022). Euxanthone inhibits lipopolysaccharide-induced injury, inflammatory response, and MUC5AC hypersecretion in human airway epithelial cells by the TLR4/MyD88 pathway. *Journal of Applied Toxicology*. DOI: 10.1002/jat.4249.

Developing a self-organized tubulogenesis model of human renal proximal tubular epithelial cells *in vitro*

Adapted from Wang X. *et al.*, 2020

Nephrotoxicity contributes to the failure of numerous drug candidates (up to 20%) in phase III clinical trials. Luminal tubule formation, or tubulogenesis, is compromised under kidney stress conditions; this is considered an early event in the development of nephrotoxicity. Renal tubules have a complex structure that supports their functions, including the reabsorption of nutrients and minerals, and secretion of urea and other waste. Renal proximal tubule epithelial cells (RPTECs) are a major component of the tubules in the human kidney. These cells have specialized brush borders and numerous mitochondria, making them highly metabolically active. RPTECs co-exist in a microenvironment containing extracellular matrix (ECM), stromal cells, and interstitial fluid. Stromal cells influence kidney morphogenesis and development. Human RPTECs grown in 3-dimensional (3D) monocultures are beginning to resemble the RPTECs' *in vivo* physiology in the tubule, but still lack the effects of the stromal cell-induced microenvironment and interactions. This article describes an improved *in vitro* human proximal tubule tissue model based on a 3D co-culture technique. Briefly, hTERT[1] immortalized human RPTECs are co-cultured on a layered ECM matrix with two types of stromal cells: murine renal fibroblasts (RFs) and human umbilical vein endothelial cells (HUVECs). The RPTECs in the 3D co-cultures developed more elongated branches and expressed multiple biomarkers in a more polarized distribution than RPTECs in 3D monocultures.

[1] Human telomerase reverse transcriptase (hTERT)

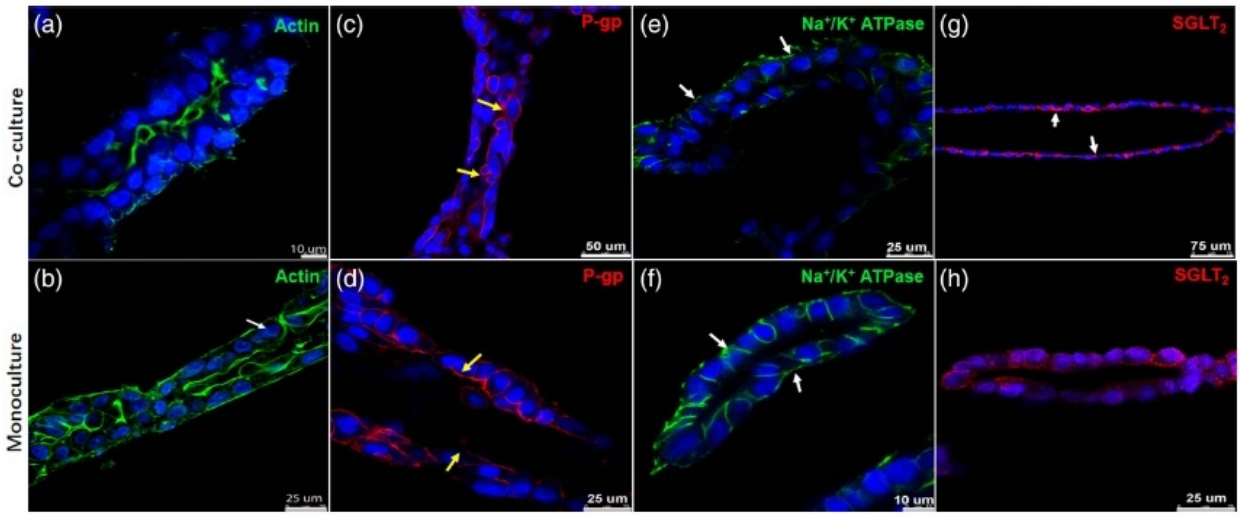

Figure 1. Immunofluorescence staining of actin, P-gp, Na^+/K^+ ATPase, and $SGLT_2$ in RPTECs grown in 3D co-cultures (top row) and 3D monocultures (bottom row). The staining of these four proteins revealed a more polarized distribution in the RPTECs grown in 3D co-cultures than those in RPTECs grown in 3D monocultures. P-gp, P-glycoprotein; RPTECs, renal proximal tubular epithelial cells; $SGLT_2$, sodium-glucose transporter 2.

Introduction

Human renal proximal tubules (PTs) play an essential role in the reabsorption and transport of nutrients from the renal filtrate to the blood. Circulating drugs and their metabolites can accumulate in these structures, resulting in nephrotoxicity; this phenomenon contributes to almost 20% of drug failures in phase III clinical trials. Detecting nephrotoxicity in its early stages can be challenging due to the presence of a large renal functional reserve, which allows the kidneys to maintain essential functions even when exposed to toxic substances. This reserve can mask the early signs of nephrotoxicity *in vivo*. The paucity of accepted biomarkers for kidney injury in humans continues to challenge clinicians in clinical trials and practice. To alleviate this challenge, researchers are pursuing the identification of sensitive biomarkers for kidney injury *in vivo* and exploring more representative *in vitro* screening methods for nephrotoxicity. Recent 3D tissue culture models more closely mimic the structural and functional aspects of RPTECs, a major component of renal tubules. Screening methods that facilitate the investigation of cellular responses to nephrotoxic agents in a more physiologically relevant manner can help elucidate the mechanisms of nephrotoxicity at early stages. These insights can assist in the development of safer pharmaceuticals and early intervention.

Recent models for tubulogenesis that use 3D organoid monocultures of human RPTECs differentiated from induced pluripotent stem cells (iPSCs) enable exploration of the early steps in the process. As described herein, co-culture of immortalized human RPTECs (RPTEC/TERT1[2], ATCC, Manassas, VA) with ECM and stromal cells more closely mimics the *in vivo* PTs than the 3D monocultures, as demonstrated by the development and longer stability of elongated branches, and more polarized distribution of multiple biomarkers.

Growth profile in 2D and 3D monocultures of RPTECs

In contrast to the cobblestone-like morphology of RPTECs in 2D culture, RPTECs in 3D monocultures began to migrate and form branch-like structures within 4-5 hours. RPTECs in 3D monocultures continued to self-assemble into longer structures although they eventually coiled, lost anchor points, and detached from the culture matrix.

Growth profile in 3D co-cultures of RPTECs and stromal cells

In 3D layer-by-layer co-culture with RFs, HUVECs, collagen, and Matrigel[2], the RPTECs showed self-assembling function and generated some elongated branch-like structures that remained much longer than those in the 3D monocultures. The metabolic activity of the RPTECs in the co-cultures significantly increased from day 1 to day 4 and then plateaued from day 4 to day 7.

Morphological characteristics

Characteristics of the *in vitro* tubular structures in the 3D monocultures and 3D co-cultures were revealed by staining for actin, P-glycoprotein (P-gp), Na^+/K^+ ATPase, and sodium-glucose transporter 2 ($SGLT_2$). The cellular distributions of these four proteins on the RPTEC membranes were more polarized in the 3D co-culture system than in the 3D monolayer culture system (Fig. 1). For example, RPTECs in the co-culture system showed a more enriched localization for P-gp staining on the apical side than the RPTECs grown in the 3D monoculture (Fig. 1c vs Fig. 1d). Similarly, Na^+/K^+ ATPase and $SGLT_2$ expression was more organized in RPTECs grown in 3D co-cultures than in

[2] CRL-4031™
[3] Matrigel ™ Corning Life Sciences

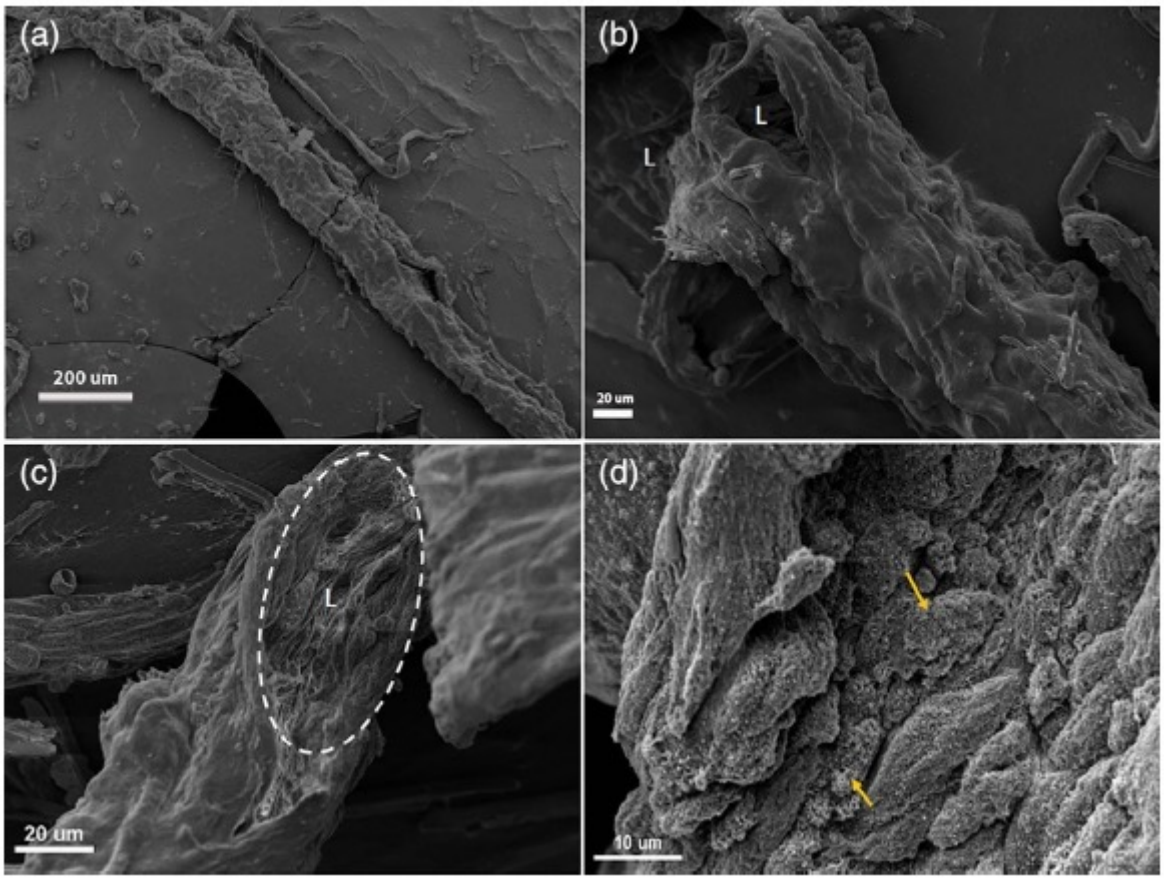

Figure 2. SEM images of co-cultured RPTECs reveal a reorganized tubule. (a) Overview; (b) smooth exterior surface of tubule with well-defined lumen structure labeled "L"; (c) rough internal surface; (d) microvilli-like structures on the internal surface. RPTECs, renal proximal tubular epithelial cells, SEM, scanning electron microscope.

RPTECs grown in 3D monocultures (Fig. 1e vs Fig. 1f and Fig. 1g vs Fig. 1h, respectively). These results suggest that the tubule structures of 3D co-cultures resemble a more physiologically relevant morphology on day 7 than the tubule structures of the 3D monocultures.

The co-cultured RPTEC tubular structures showed a well-defined lumen with a rough internal surface and a smooth exterior surface in the images taken by a scanning electron microscope (SEM) (Fig. 2). SEM images of the internal surface revealed the formation of some microvilli-like structures (Fig. 2d).

Proliferative activity

The average percentage of RPTECs undergoing proliferation decreased significantly from day 1 (>20%) to day 3 (< 5%) in both the 3D co-cultures and 3D monocultures. In contrast, the average percentage of the RPTECs grown in 2D monolayer culture at day 3 remained high (>20%), indicating that the different culture conditions profoundly influenced the proliferative state of the RPTECs.

Gene expression of RPTECs under different culture conditions

The effects of the three different culture conditions on the day-7 expression of 10 genes involved in functional differentiation of RPTECs were determined by quantitative real-time PCR analysis (qRT-PCR, Fig. 3). In comparison to RPTECs grown in 2D monolayers, the RPTECS grown in the 3D monocultures and 3D co-cultures exhibited significantly higher expression of mRNA transcripts for 4 and 10 functional genes, respectively (*$p<0.05$). Furthermore, the RPTECs in the 3D co-cultures displayed significantly higher transcript expression for 9 genes (except ABCb1) as compared to the RPTECs grown in 3D monocultures (Fig. 3).

Summary

This study presented 3D co-culture conditions for hTERT-immortalized RPTECs that resulted in the cells developing self-organized tubules and showing improved tubular tissue-like characteristics including viability; functional gene expression; morphology; polarized distribution of P-gp, Na^+/K^+ ATPase, and $SGLT_2$; and reduced proliferative activity. The layer-by-layer culture matrices include two types of stromal cells (HUVECs

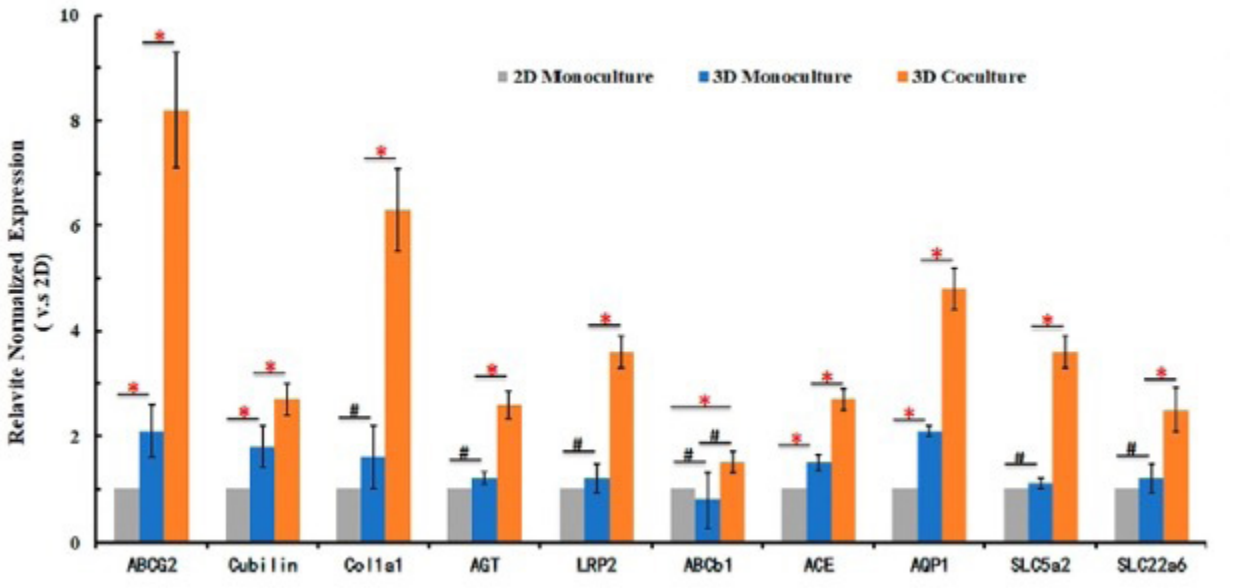

Figure 3. Transcript expression profiles of ten functional genes of RPTECs grown under different culture conditions as determined by quantitative real-time PCR. The RPTECs in the 3D culture conditions (monoculture and co-cultures) exhibited higher transcript levels for 4 and 10 functional genes, respectively, as compared to those grown in 2D monocultures. Data are reported as mean ± S.D. of three replicates after normalized to the Ct value of GAPDH. *p<0.05, #p>0.05. ABCG2, ATP-binding cassette (ABC) transporter subfamily G member 2; Col1a1, collagen type 1 alpha-1; AGT, angiotensinogen; LRP2, low-density lipoprotein receptor-related protein 2; ABCb1 ATP-binding cassette (ABC) transporter subfamily B member 1; ACE, angiotensin-converting enzyme; AQP1, aquaporin 1; SLC5a2, sodium-glucose co-transporter 2; SLC22a6, solute carrier family 22 member 6, also known as OAT1 (organic anion transporter 1); S.D., standard deviation.

and murine renal fibroblasts) and Matrigel, which contains not only collagen 1 but also additional types of glycosaminoglycans and ECM proteins. This RPTEC 3D co-culture technique used a commercially available immortalized human RPTEC cell line (RPTEC/TERT1, ATCC, CRL-4031) and readily available stromal cells, so the technique is reproducible. A major advantage of this human RPTEC 3D co-culture technique includes the partial recreation of the native microenvironment of renal proximal epithelial cells *in vitro*.

This improved *in vitro* model of tubulogenesis can support further exploration of the functions of relevant genes and the mechanisms controlling luminal polarization. In addition, this *in vitro* human tubulogenesis 3D co-culture model may be used to elucidate the underlying mechanisms of nephrotoxicity of known drugs and may function as a screening tool for potential nephrotoxicity of drug candidates.

APPLICATION NOTE

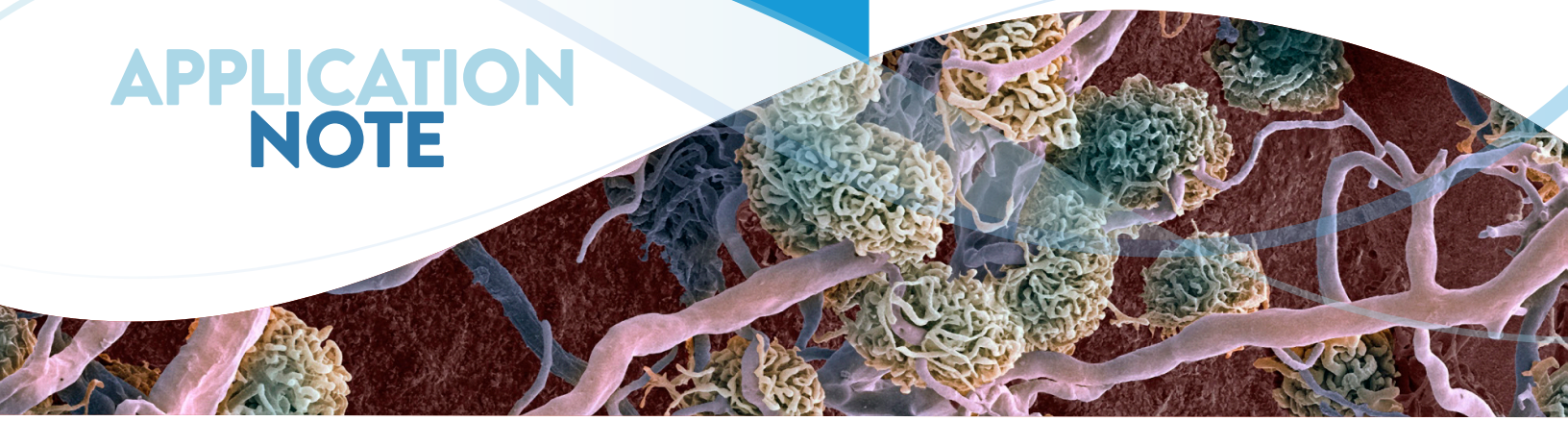

GENETICALLY MODIFIED RENAL PROXIMAL TUBULE EPITHELIAL CELLS

A PHYSIOLOGICALLY RELEVANT RENAL SOLUTE CARRIER UPTAKE MODEL FOR DRUG TOXICITY STUDIES

Chaozhong Zou, PhD*; Luis Romero, MS*; Elizabeth Turner, PhD*; Brian A. Shapiro, PhD†; Penney McWilliams-Koeppen, MS*; and Brian Chase, MS†

*ATCC Cell Systems, Gaithersburg, MD 20877

†ATCC, Manassas, VA 20110

ABSTRACT

Solute carrier kidney transporter (SLC) protein models are essential for determining the renal clearance of drugs, environmental compounds, and endogenous molecules. However, to date there is a lack of preclinical cell-based models; many current models do not express critical SLC proteins and those that do are not of mature adult kidney tissue origin. We created three different hTERT-immortalized human primary renal proximal tubule epithelial cells (RPTEC) that stably express the OAT1, OCT2, and OAT3 proteins. We then tested the ability of these cells to intracellularly convey known SLC protein substrates.

INTRODUCTION

The disposition and clearance of drugs by the kidney relies largely on a well-characterized subset of membrane transport pumps that are collectively known as solute carrier or SLC proteins.[1,3] SLC transporters are membrane proteins that use a variety of energy-coupling mechanisms to transport solutes, such as ions, metabolites, peptides, and drugs, across biological membranes. Among the SLC family proteins, OAT1 (SLC22A6), OCT2 (SLC22A2), and OAT3 (SLC22A8) are the most important transporters in kidney tissue. Because the activity of these pumps is often the limiting factor for solute clearance from the kidney, they are recommended by both the US Food and Drug Administration[1] (FDA) and the European Medicines Agency (EMA) as targets for drug-drug interaction studies. There is therefore a need for kidney toxicity models, especially in vitro models, that have human kidney origination, functioning transporters, accurate clinical predictability, and consistent data output for initial drug interaction studies.

Unfortunately, primary renal epithelial cells lose OAT1, OCT2, and OAT3 transporter expression quickly once placed in culture. Transiently expressing these transporters in primary renal epithelial cells yields large variations between production lots, making the data from those experiments hard to interpret. In addition to the transiently expressed SLC protein models, there are cell line-based models of kidney transporter function such as MDCK, CHO, and U2OS. Due to the fact that they may not have human kidney tissue origination or are themselves cancer lines, these models may significantly compromise clinical predictability. During the course of this project we generated kidney transporter cell models using well-characterized hTERT-immortalized RPTEC[2] (RPTEC/TERT1, ATCC® CRL-4031™) that stably overexpress the OAT1, OCT2, or OAT3 gene. After confirming the SLC mRNA expression of each gene by RT-PCR, we performed immunostaining to confirm that OAT1, OCT2, and OAT3 are correctly trafficked to the plasma membrane. Notably, those clones show typical epithelial

morphology and express the appropriate epithelial markers. Most importantly, we have verified that the overexpressed transporters have normal transport activities using 6-CF (6-carboxyfluorescein) or EAM-1 (N,N,N-Trimethyl-2[(7-nitro-1,2,3- benzoxadiazol-4-yl)amino] ethanaminium iodide) uptake assays. Furthermore, uptake of these compounds can be inhibited in a dose-dependent manner by well-known SLC inhibitors, indicating that the overexpressed kidney transporters are functioning as expected. Overall, our data demonstrate that these modified renal epithelial cell lines maintain kidney transporter expression over time, are useful tools that provide physiologically relevant data regarding human kidney function, and are more consistent and reliable than comparable in vitro models currently used in clinical trials determining the effect of exogenous compounds on renal membrane transporter function.

MATERIALS AND METHODS

RPTEC/TERT1 (ATCC CRL-4031™) were transfected with a plasmid expressing the full-length sequence of human OAT1, OCT2, or OAT3. The genetically modified cells were grown under antibiotic selection and individual positive clones were identified and verified by RT-PCR, immunofluorescence, and Sanger sequencing (Figure 1). The parental line was used as a control. A single clone, positive for each SLC transporter, was selected for further validation based upon optimal results from the assays. Cell culture medium consisted of DMEM: F-12 Medium (ATCC 30-2006™) supplemented with hTERT Immortalized RPTEC Growth Kit (ATCC ACS-4007™). OAT1, OCT2, and OAT3 transfectants were seeded onto poly-L-ornithine-coated chamber slides and cultured at 37°C, 5% CO_2. After 24 hours, the OAT1-expressing cells were fixed and stained with a mouse monoclonal antibody against OAT1 (Abcam) and a goat anti-mouse 596 secondary antibody then visualized with a fluorescent microscope. The fixed OCT2-expressing cells were stained with a rabbit polyclonal antibody against OCT2 (Millipore) and a goat anti-rabbit 488 secondary antibody. The fixed OAT3-expressing cells were stained with a rabbit polyclonal antibody against OAT3 (GeneTex) and a goat anti-rabbit 488 secondary antibody. Cell micrographs were acquired using an Eclipse Ti inverted microscope (Nikon) and a Zyla sCMOS camera (Andor). Sanger sequencing confirmed that the resulting RPTEC/TERT1-OAT1 (ATCC CRL-4031-OAT1™), RPTEC/TERT1-OCT2 (ATCC CRL-4031-OCT2™), and RPTEC/TERT1-OAT3 (ATCC CRL-4031-OAT3™) lines expressed the appropriate SLC gene with no mutations. Western blot analysis further confirmed the presence of the appropriate SLC protein in the OAT1- and OCT2-transfected clones. Digital PCR confirmed that RPTEC/TERT1-OAT1 has 7 copies of the OAT1 gene, RPTEC/TERT1-OCT2 has 5 copies of the OCT2 gene, and RPTEC/TERT1-OAT3 has 5 copies of the OAT3 gene (data not shown).

For the uptake assays, OAT1-expressing cells, OAT3-expressing cells, or control cells were seeded at 1 x 10^5 cells/well in black-walled, collagen-coated 96-well plates. After 24 hours, the cells were washed in prewarmed Hank's Balanced Salt Solution (HBSS) (ATCC 30-2213™), followed by a 10-minute incubation in HBSS at 37°C, 5% CO_2. Cells were then incubated with 3 µM 6-CF (Thermo Fisher Scientific) for 20 minutes at 37°C, 5% CO_2. After incubation, the reaction was terminated by washing the cells 4 times with cold HBSS. Cells were then lysed with M-Per Mam*mali*an Protein Extraction Reagent (Thermo Fisher Scientific) and read immediately on a fluorescent plate reader at 490ex/530em or visualized by fluorescent microscopy. The OCT2 assay experiments were conducted in the same manner as the OAT1 and OAT3 assays with the exception of the substrate, which was 5 µM EAM-1. For the inhibition assays, OAT1-, OCT2-, or OAT3-expressing cells were incubated with the appropriate uptake chromophore. For OAT1- and OAT3-expressing clones, cells were incubated with varying concentrations of either probenecid (Sigma) or novobiocin (Sigma) for 10 minutes in 96-well plates, and then uptake was measured as described above. For OCT2-expressing clones, the cells were incubated with varying concentrations of either cimetidine (Sigma) or quinitin (Sigma) for 20 minutes in 96-well plates, and then uptake was measured as described above.

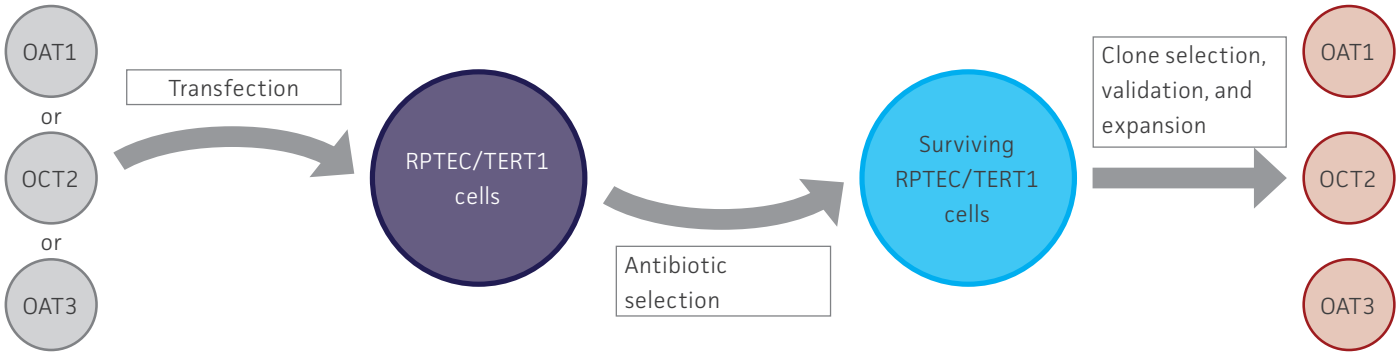

Figure 1: Generation of stably overexpressing OAT1, OCT2, and OAT3 RPTEC/TERT1 cell lines. RPTEC/TERT1 cells were transfected with plasmid DNA constructs containing either OAT1, OCT2, or OAT3. After 24 hours, transfected cells were grown under antibiotic selection for 7 days. The surviving cells were subjected to clonal isolation and were then expanded. The isolated clones were validated for clonality, kidney transporter expression, and kidney transporter activity.

RESULTS

We confirmed the expression of OAT1, OCT2, or OAT3 in RPTEC/TERT1 by RT-PCR. The expression of OAT1 or OCT2 was verified by western blot. In addition, immunofluorescence revealed that the cells were positive for membrane-localized OAT1, OCT2, or OAT3 (Figure 2). Further, the clonal OAT1, OCT2, or OAT3 cells retain important characteristics of the parental counterpart RPTEC/TERT1 cell; dome formation and normal expression of CD13 and E-cadherin were observed in OAT1, OCT2, and OAT3 positive clones (Figure 3).

Next, we tested the ability of OAT1- and OAT3-expressing clones to uptake 6-CF, a known substrate of OAT1 and OAT3. We observed significant uptake ratios relative to the parental cells. Further, the uptake activity of OAT1- and OAT3-expressing clones was observed to be dose dependent (Figure 4). Similarly, we tested OCT2-expressing cells to uptake EAM-1, a known substrate of OCT2. As in the OAT1- and OAT3-expressing cells, we observed significant, concentration-dependent uptake ratios in OCT2-expressing cells relative to the parental cells (Figure 4).

We then tested the ability of various organic ion transporter inhibitors to block substrate transport into OAT1, OCT2, and OAT3-expressing cells. We observed that the compounds probenecid and novobiocin were able to block 6-CF (Probenecid: IC_{50}=16.91 µM; novobiocin: IC_{50}=59.17 µM) transport into RPTEC/TERT1-OAT1 (Figure 5). Similarly, probenecid and novobiocin blocked 6-CF (Probenecid: IC_{50}=49.02µM; novobiocin: IC_{50}=70.90 µM) uptake into RPTEC/TERT1-OAT3 (Figure 5). In the same regard, the compounds cimentidine and quintinin were able to block EAM-1 (Cimentidine: IC_{50}=93.5 µM; quintinin: IC_{50}=59.5 µM) entry into RPTEC/TERT1-OCT2 (Figure 5). The IC_{50} values that were observed in these experiments were similar to those reported in other competitive inhibition studies using the test compounds.[4-8]

Over the course of this project we generated and tested 3 new hTERT-immortalized, renal SLC protein models.

The new cell models displayed:

- Appropriate transporter protein expression and localization
- Key proximal tubule cell biologies
- Potent and specific transporter activity

Thus, these new SLC protein-expressing cell models are robust tools for toxicological testing.

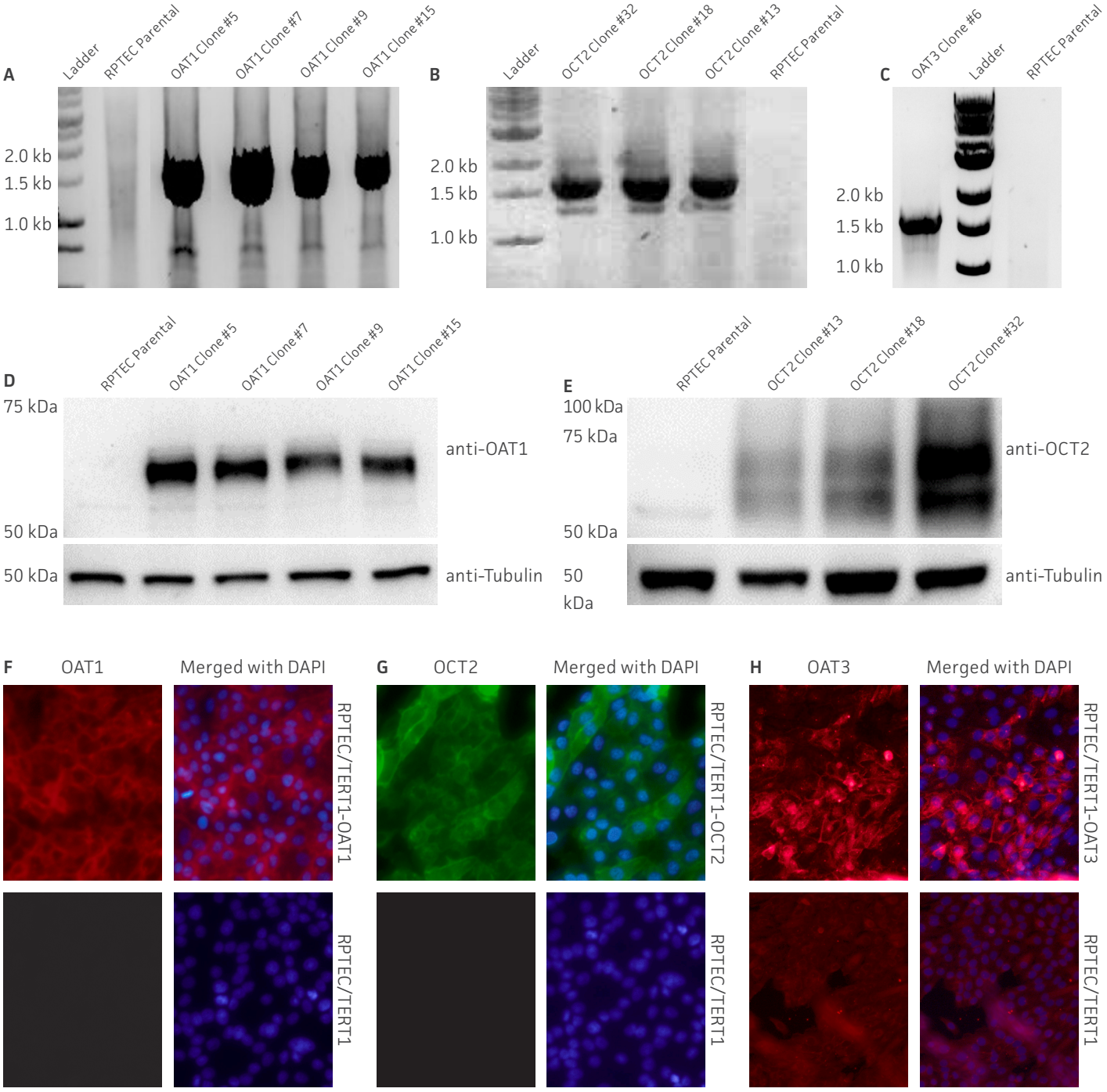

Figure 2: Characterization of the RPTEC/TERT1 SLC transporter cells. RT-PCR data demonstrates the presence of OAT1 (A), OCT2 (B), or OAT3 (C) mRNA in the respective cell lines. Immunoblot demonstrates the presence of OAT1 (D) and OCT2 (E) protein expression in the respective cell lines. Immunofluorescence demonstrates expression and plasma membrane localization OAT1 (F), OCT2 (G), or OAT3 (H), in the respective cell lines, but not the parental line. Original magnification, x20.

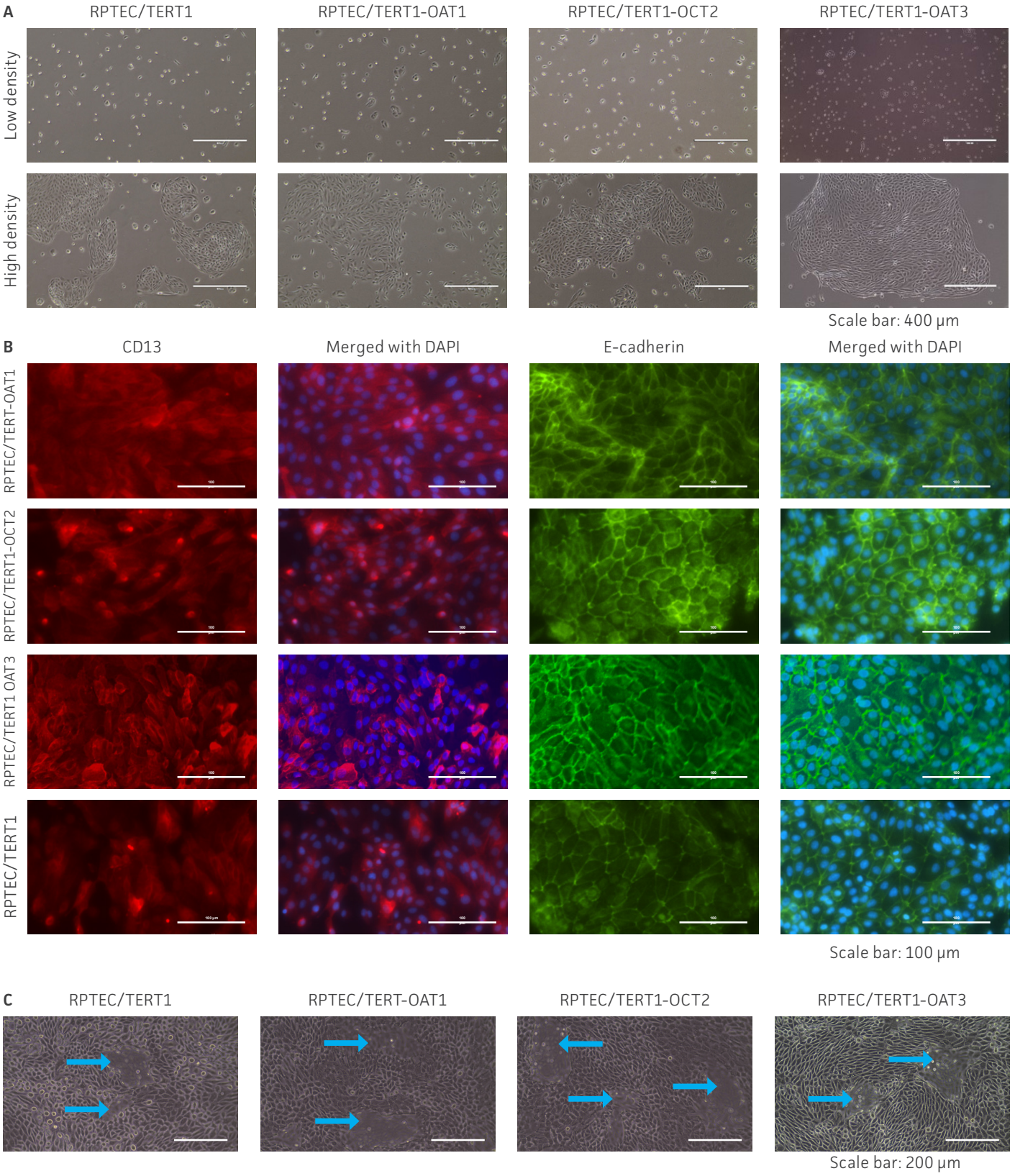

Figure 3: The RPTEC/TERT1 transporter cells retain the most important characteristics of the parental cells. RPTEC/TERT1 SLC transporter cells were subjected to immunostaining and dome formation assays. A) OAT1, OCT2, and OAT3 clones display the same renal epithelial growth pattern as parental RPTEC/TERT1 cells. B) The renal epithelial markers CD13 and E-cadherin are expressed in both parental RPTEC/TERT1 cells and in the OAT1, OCT2, and OAT3 lines. C) Dome formation is not compromised in OAT1-, OCT2-, and OAT3- expressing cells, as demonstrated by the formation of dome-like structures (arrows) caused by solute transport across an intact epithelial barrier.

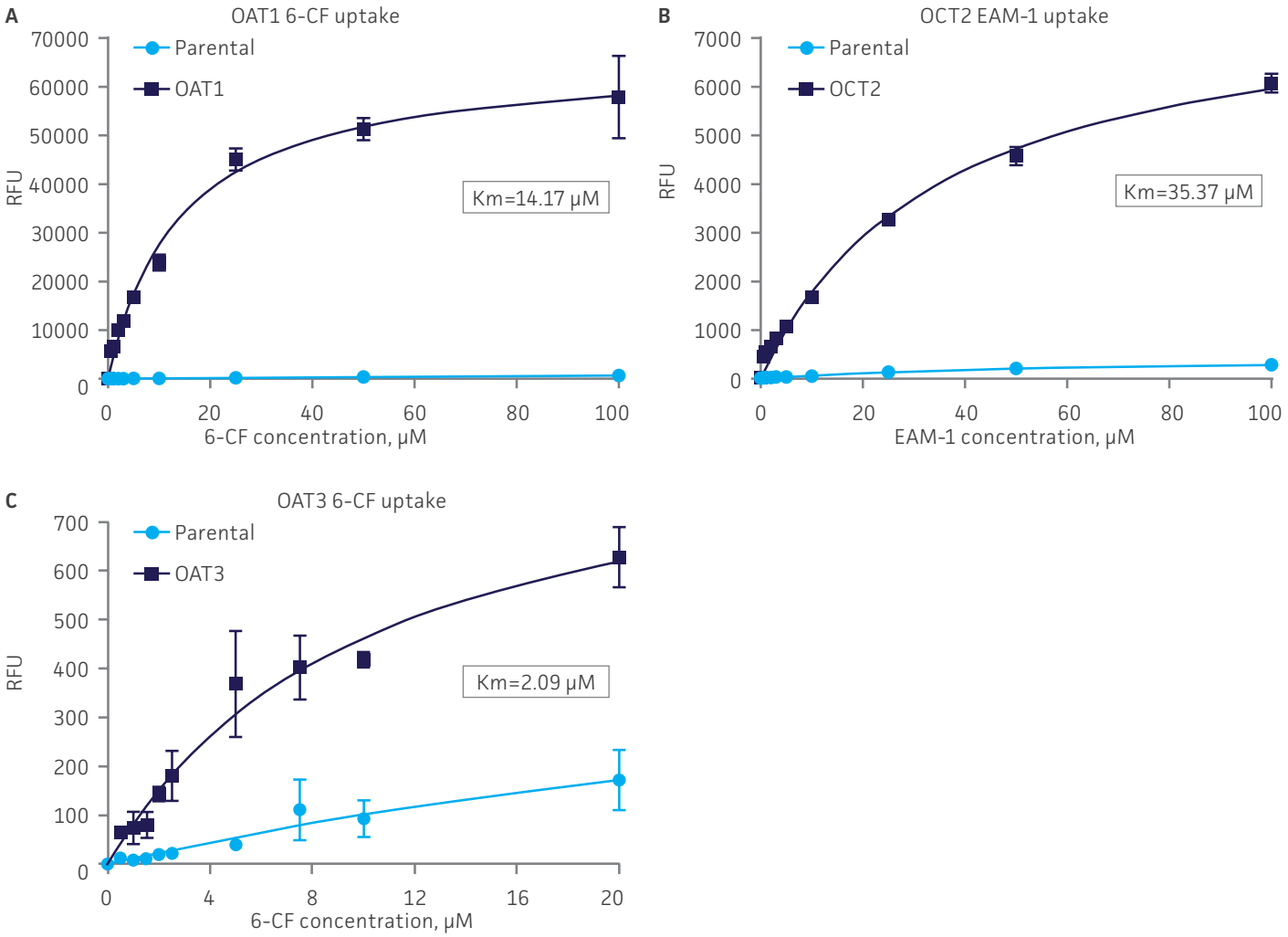

Figure 4: SLC transporter-expressing cells display potent substrate uptake activity. Solute uptake activity of (A) OAT1- and (C) OAT3-expressing cells was assessed using 6-CF as a substrate. Solute uptake activity of (B) OCT-2 was assessed using EAM-1 as a substrate. As expected, uptake increases with increasing substrate concentration in solute transporter-expressing cells but not in parental RPTEC/TERT1 cells (n=3; error bars indicate standard deviation), indicating that the observed transport is due to OAT1, OCT2, or OAT3 expression.

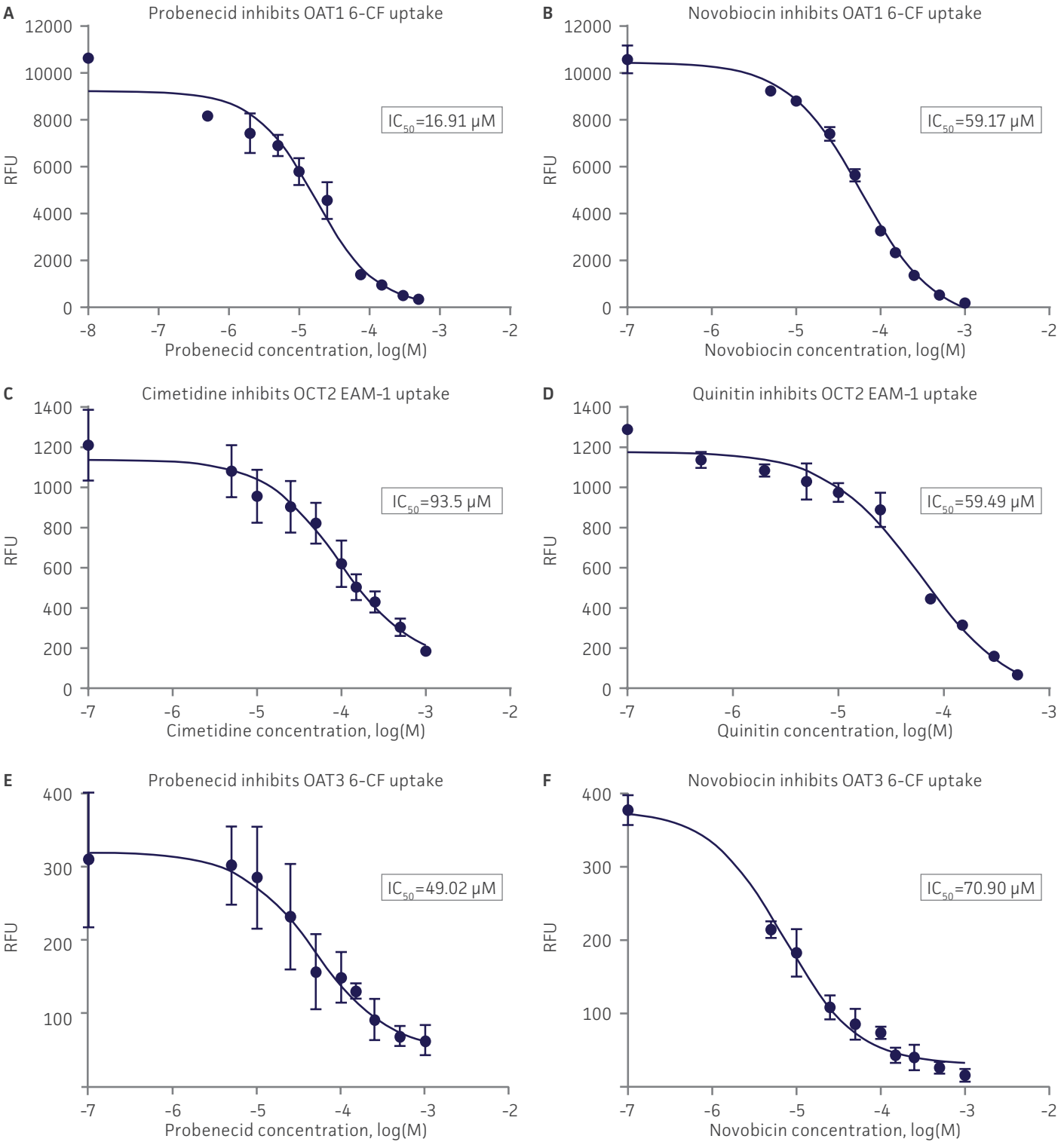

Figure 5: SLC transporter-expressing cells demonstrate highly specific uptake activities. OAT1-expressing cells were exposed to increasing concentrations of the known OAT inhibitors A) probenecid and B) novobiocin while 6-CF concentration and uptake time were held constant at 3 µM and 20 minutes, respectively. OCT2-expressing cells were exposed to increasing concentrations of the known OCT2 inhibitors C) cimetidine and D) quinitin while EAM-1 concentration and uptake time were held constant at 5 µM and 20 minutes, respectively. OAT3-expressing cells were exposed to increasing concentrations of the known OAT inhibitors E) probenecid and F) novobicin while 6-CF concentration and uptake time were held constant at 3 µM and 20 minutes, respectively. The resulting inhibition curves indicate that OAT1, OCT2, and OAT3 transport activity was substrate specific when overexpressed in RPTEC/TERT1 cells (n=3; error bars indicate standard deviation).

BACK TO CONTENTS

SUMMARY AND CONCLUSIONS

A central problem in preclinical studies is the lack of models that display key features of the kidney, such as the renal microenvironment and expression of the appropriate SLC proteins. In this regard, we have generated and characterized cellular models for renal solute uptake by stably expressing OAT1, OCT2, and OAT3 in hTERT-immortalized human primary RPTEC/TERT1. The OAT1-, OCT2-, and OAT3-overexpressing cells retained the relevant renal epithelial characteristics of the parental primary cells, and stable transporter expression was confirmed by PCR, immunostaining, and immunoblot. All 3 cell models showed highly sensitive and specific substrate uptake activities, making them valuable tools for drug-drug interaction studies and/or preclinical toxicology testing to support clinical therapeutic development. Further, the transport activity in all 3 cell models was inhibited by known SLC inhibitors such as probenecid, quintin, novobiocin, and cimetidine. Thus, the proliferative capacity, in vivo-like qualities, and substrate sensitivity and specificity of RPTEC/TERT1-OAT1, -OCT2, and -OAT3 establish these cells as valuable, physiologically relevant models of kidney function.

REFERENCES

1 Guidance for Industry: Drug Interaction Studies-Study Design, Data Analysis, Implications for Dosing, and Labeling Recommendations. US Food and Drug Administration. Feb, 2012.

2 Wieser M, et al. hTERT alone immortalizes epithelial cells of renal proximal tubules without changing their functional characteristics. Am J Physiol-Renal Physiol 295: F1365–F1375, 2008.

3 The International Transporter Consortium. Membrane transporters in drug development Nat Rev Drug Disc. 9: 215-235, 2010.

4 Ho ES, et al. Cytotoxicity of antiviral nucleotides adefovir and cidofovir is induced by the expression of human renal organic anion transporter 1. J Am Soc Nephrol 11(3) : 383-93, 2000. PubMed : 10703662

5 Takeda M, et al. Characterization of organic anion transport inhibitors using cells stably expressing human organic anion transporters. Eur J Pharmacol. 419(2-3):113-20, 2001. PubMed : 11426832

6 Chu XY, et al. Transport of the dipeptidyl peptidase-4 inhibitor sitagliptin by human organic anion transporter 3, organic anion transporting polypeptide 4C1, and multidrug resistance P-glycoprotein. J Pharmacol Exp Ther 321(2):673-83, 2007. PubMed: 17314201

7 Zolk O, et al. Structural determinants of inhibitor interaction with the human organic cation transporter OCT2 (SLC22A2). Naunyn Schmiedebergs Arch Pharmacol. 379(4):337-48, 2009. PubMed: 19002438

8 Ito S, et al. Competitive inhibition of the luminal efflux by multidrug and toxin extrusions, but not basolateral uptake by organic cation transporter 2, is the likely mechanism underlying the pharmacokinetic drug-drug interactions caused by cimetidine in the kidney. J Pharmacol Exp Ther 340(2):393-403, 2012. PubMed: 22072731

10801 University Boulevard
Manassas, Virginia 20110-2209

703.365.2700 703.365.2701 sales@atcc.org www.atcc.org

AP-112021-v06

Euxanthone inhibits lipopolysaccharide-induced injury, inflammatory response, and MUC5AC hypersecretion in human airway epithelial cells by the TLR4/MyD88 pathway

Adapted from Shen W. *et al.*, 2022

Asthma progression involves airway inflammatory responses, dysfunction of airway epithelial cells (AECs), airway remodeling, and hypersecretion of mucus. Euxanthone, a plant-derived xanthone, has been found to exhibit cytotoxic activity against several human diseases. Because its parent plant is used for alleviating cough symptoms, this study investigated the effect of euxanthone on injured AECs. Network pharmacology analysis revealed that euxanthone may modulate the lipopolysaccharide (LPS)-induced responses of AECs. Exposure of the BAES-2B and 16HBE airway epithelial cell lines with LPS resulted in reduced cell viability, augmented apoptosis and lactate dehydrogenase (LDH) release, and increased secretion of inflammatory cytokines and MUC5AC glycoprotein. Simultaneous treatment of the AECs with euxanthone inhibited LPS-induced injury, inflammatory responses, and hypersecretion of mucus. Further experiments indicated that euxanthone's mechanism of action involved modulation of the TLR4/MyD88 pathway.

Introduction

AECs play a critical role in asthma and provide the frontline of defense against respiratory pathogens and exogenous toxic particles. LPS, a component found on the outer membrane of gram-negative bacteria, is a common etiological agent of asthma. LPS stimulation of AECs can trigger inflammatory cascades and lead to AEC dysfunction. The prevalence and mortality of pediatric asthma are increasing despite newer medications and public health initiatives. Thus, developing new treatments for asthma is necessary.

Euxanthone, a flavonoid found in the roots of the medicinal plant *Polygala caudata*, has been used as a remedy for anxiety and coughs for centuries. Although its anti-cancer effects and modulation of several neurological disorders are documented, euxanthone's effect on asthma remains unexplored. Network pharmacology analysis clarifies the interrelationships of diseases, drugs, and drug targets, and is especially useful for elucidating the pharmacology of compounds that modulate multiple targets. This study used network pharmacology analysis to determine probable mechanisms of euxanthone against asthma and its underlying processes. The hypothesized mechanisms of euxanthone were evaluated in LPS-induced injury of human AECs as an *in vitro* asthmatic model.

Network pharmacology analysis

A comparison of euxanthone-related targets and asthma-associated targets in DisGeNet and GeneCards revealed 14 overlapping targets. GO analysis indicated that these 14 candidate targets were associated with regulating cytokine production in inflammatory responses and cellular responses to LPS. Kegg pathway enrichment analysis suggested the involvement of the signaling pathways for toll-like receptors (TLR), T cell receptors, and tumor necrosis factor (TNF).

Effect of euxanthone on LPS-induced injury in human AECs

A dose-response curve showed that euxanthone treatment at concentrations up to 20 μM had no significant effect on the viability of the human airway epithelial cell lines BEAS-2B[1] (ATCC) and 16HBE (Fig. 1A, B). LPS exposure of BEAS-2B and 16HBE AECs significantly reduced viability and increased LDH production, whereas co-treatment with 20 μM euxanthone significantly diminished the LPS-induced injury (Fig. 1C-F). Furthermore, LPS exposure also increased the percentage of AECs undergoing cell death by apoptosis, which was significantly alleviated by co-treatment with euxanthone (Fig. 1G, H).

Effect of euxanthone on LPS-induced inflammatory response

LPS treatment increases the production and secretion of the inflammatory cytokines interleukin 6 (IL-6), IL-8, and monocyte chemoattractant protein-1 (MCP-1) from AECs after 24 hrs. Co-treatment of BEAS-2B and 16HBE with LPS and 20 μM euxanthone significantly attenuated the production of these inflammatory cytokines. These results indicate that euxanthone co-treatment of AECs significantly inhibited LPS-induced inflammatory cytokine production.

Effect of euxanthone on LPS-induced hypersecretion of mucus protein MUC5AC in AECs

MUC5AC is a heavily glycosylated protein in mucus and can be produced by AECs. LPS treatment increases production and secretion

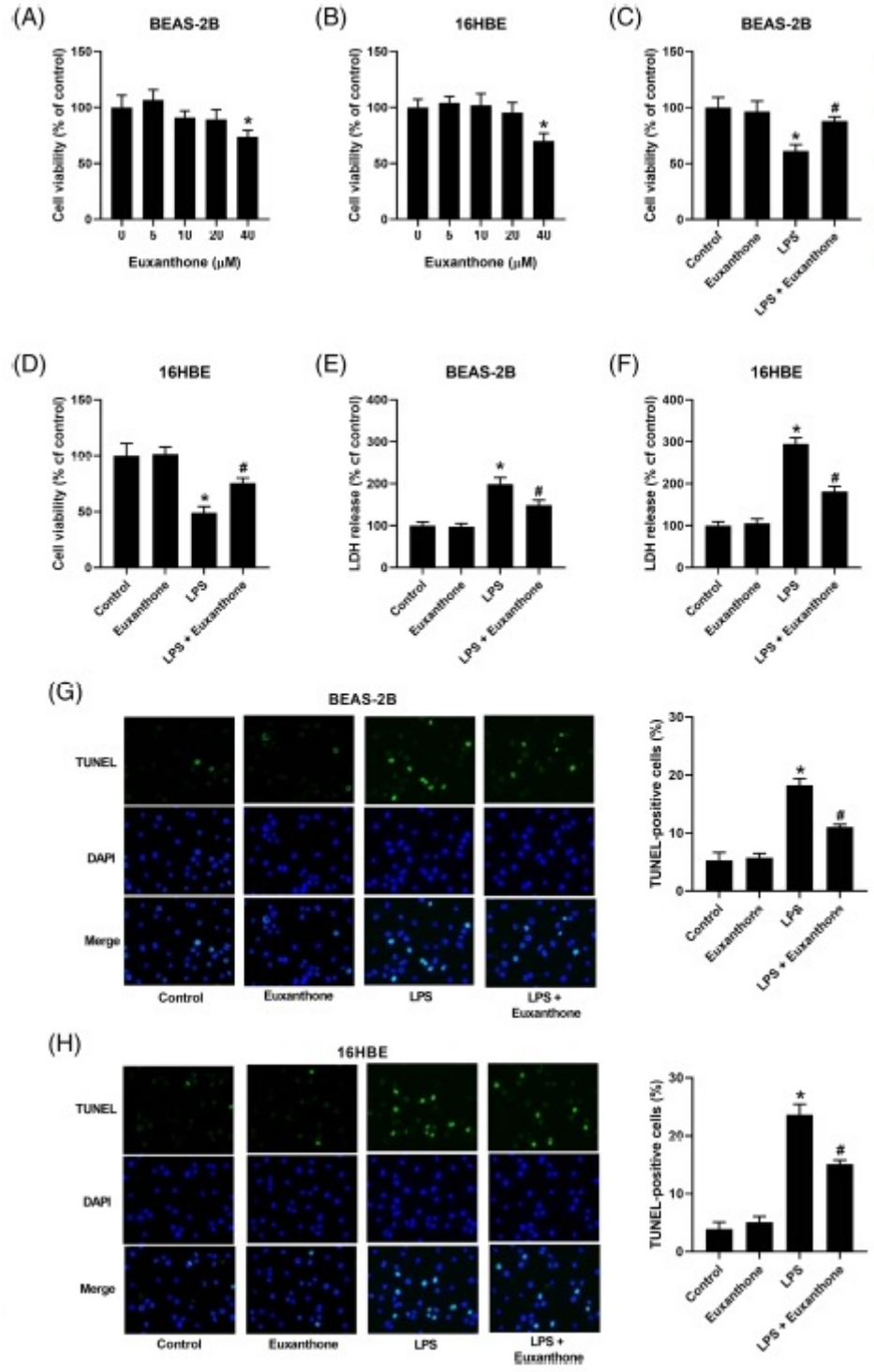

Figure 1. Euxanthone diminished LPS-induced injury of AECs. (A, B) Dose-response curve of euxanthone on cell viability of BEAS-2B or 16HBE cells after 24 hrs as determined by the CCK-8 assay. (C-H) BEAS-2B and 16HBE cells were treated with 5 μg/mL LPS, 20 μM euxanthone, or both. After 24 hrs, cell viability was measured by (C, D) CCK-8 assay, (E, F) LDH release, or (G, H) TUNEL assay. Results presented as mean ± S.D. Statistical significance was set at P<0.05; *P<0.05 vs control, #P<0.05 vs LPS. LPS, lipopolysaccharide; S.D., standard deviation; TUNEL, terminal deoxynucleotidyl transferase-mediated dUTP nick end-labeling

[1] CRL-3588 ™

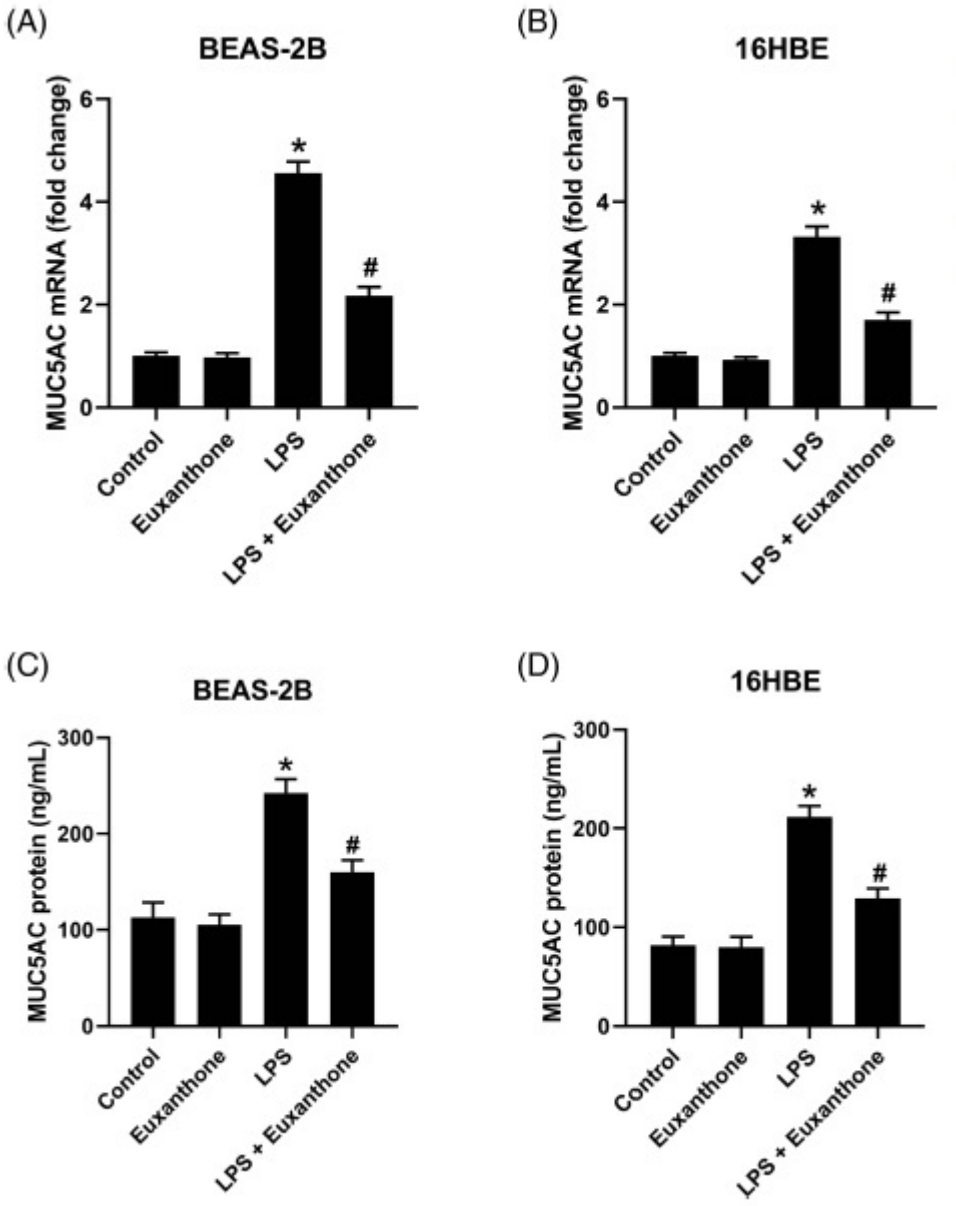

Figure 2. Euxanthone suppressed LPS-induced hypersecretion of MUC5AC in AECs. BEAS-2B or 16HBE cells were treated with LPS and/or 20 μM euxanthone for 24 hrs. (A, B) Cells were harvested and the MUC5AC mRNA transcripts were quantified by qRT-PCR. (C, D) MUC5AC proteins in cell supernatants were measured with a commercially available ELISA kit. Results are expressed as mean ± S.D. *P<0.05 vs control, P<0.05 vs LPS. ELISA, enzyme-linked immunosorbent assay; qRT-PCR, quantitative real-time PCR.

of the MUC5AC glycoprotein from AECs after 24 hrs, as shown by an increase in both MUC5AC mRNA levels (Fig. 2A, B) and MUC5AC protein levels in the supernatant (Fig. 2C, D). Co-treatment of the BEAS-2B and 16HBE AECs with LPS and 20 μM euxanthone significantly inhibited LPS-induced MUC5AC production (Fig. 2A-D). Euxanthone significantly suppressed the LPS-induced rise in MUC5AC mRNA levels and the quantity of secreted glycoprotein in the cell supernatant, suggesting that euxanthone may thwart LPS activation of specific genes.

Effect of euxanthone on TLR4/MyD88 pathway in LPS-stimulated human AECs

The TLR4/MyD88 (toll-like receptor 4/myeloid differentiation factor 88) pathway participates in regulating inflammation and immune responses. MyD88 is a key adapter for TLR4. Higher expression of TLR2, TLR3, and TLR4 and activation of the TLR4 pathway are associated with severe asthma. The effect of euxanthone on the TLR4/MY88 pathway was investigated by assessing any changes in expression with western blot analysis (Fig. 3). LPS stimulation significantly augmented the expression of TLR4 and MyD88 proteins in BEAS-2B (Fig. 3A-C) and 16HBE cells (Fig. 3D-F). Euxanthone treatment significantly inhibited LPS-induced activation of the TLR4/MY88 pathway in both human AECs (Fig. 3), indicating that blocking TLR4/MyD88 activation is a molecular mechanism of euxanthone.

TLR4 knockdown enhanced the effect of euxanthone on LPS-induced injury, inflammatory response, and MUC5AC hypersecretion in human AECs

Using si-TLR4 (small interference RNA against TLR4) transfection to inhibit the pathway, it was found that euxanthone inhibited the expression of TLR4 in response to LPS. Additionally, treatment with euxanthone reduced LDH release, apoptosis, and secretion of IL-6, IL-8, MCP-1, and MUC5AC, while transfection with TLR4 further enhanced these effects. These findings suggest that euxanthone can mitigate LPS-induced injury, inflammatory response, and MUC5AC hypersecretion in human AECs by inhibiting the TLR4/MyD88 pathway.

Summary

These results indicate that euxanthone modulates the effects of LPS on AECs, at least partially through its inhibition of the TLR4/MyD88 pathway. The BEAS-2B airway epithelial cell line enables researchers to elucidate the effects of a compound (euxanthone) on LPS-induced injury as an *in vitro* model of asthma. The commercial availability of this cell line in addition to the accessibility of well-established conditions for culturing adds to the ease of establishing a relevant *in vitro* model for asthma epithelial cells and provides reproducible results for probing the mechanisms of action for promising compounds.

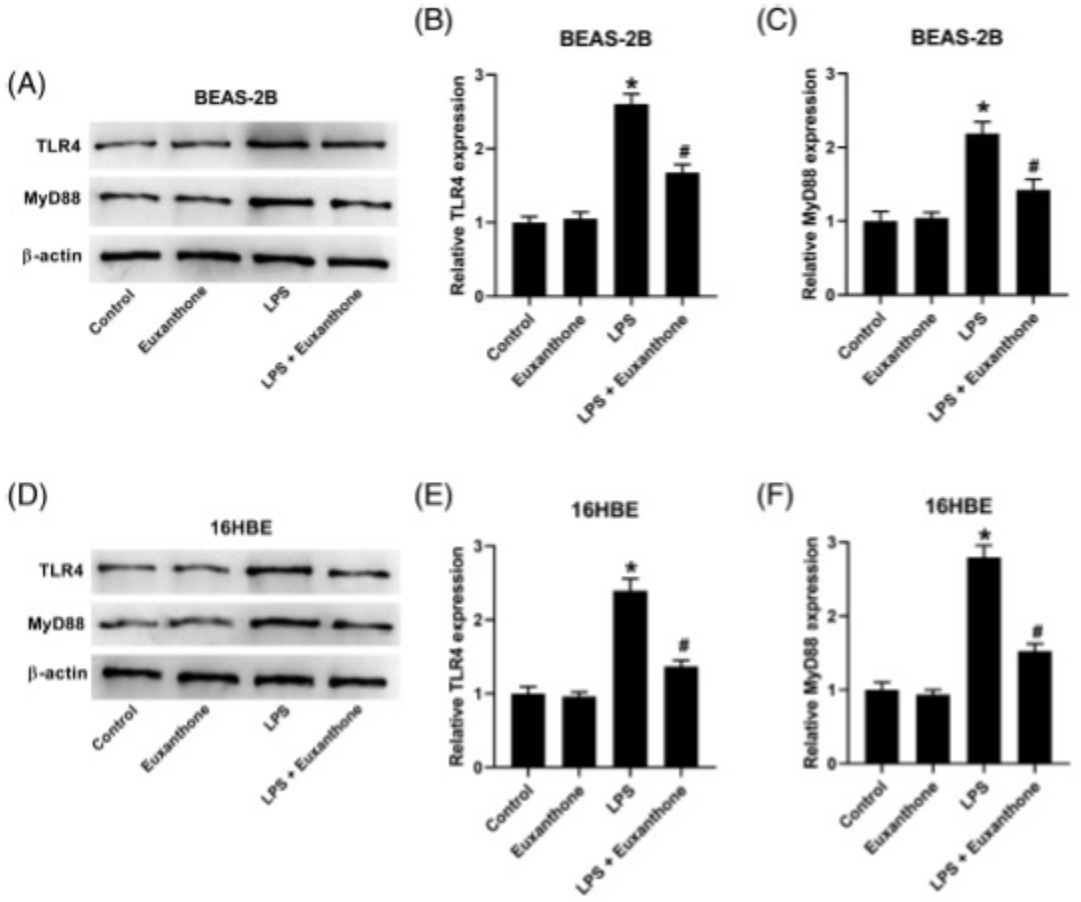

Figure 3. Euxanthone significantly weakened the LPS-induced activation of the TLR4/MyD88 pathway in human AECs. BEAS-2B and 16HBE cells were exposed to 5 μg LPS and/or 20 μM euxanthone for 24 hrs. The expression levels of TLR4 and MyD88 in BEAS-2B and 16HBEcells were determined by western blot analysis. *P<0.05 vs control, #P<0.05 vs LPS. MyD88, myeloid differentiation factor 88; TLR4, toll-like receptor 4.

APPLICATION NOTE

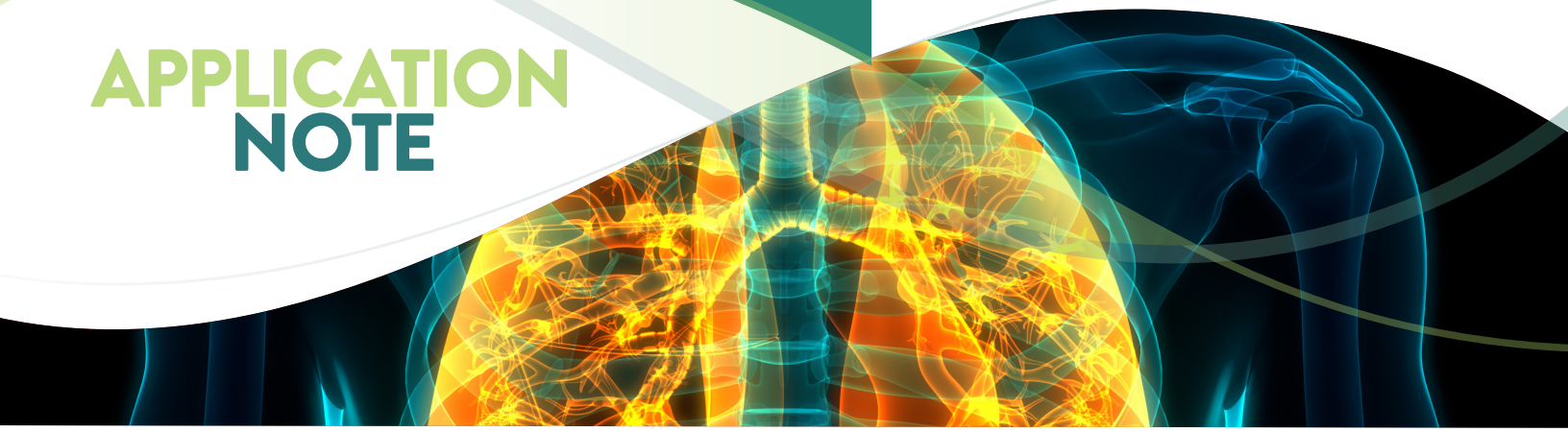

COMPARING TOXICOLOGICAL RESPONSES BETWEEN ALI-INCUBATED PRIMARY AIRWAY EPITHELIAL CELLS AND UNDIFFERENTIATED COUNTERPARTS

Kevin Tyo, PhD

Respiratory tract diseases stemming from inhalation exposure of toxic compounds significantly contributes to the global health burden. Traditional in vitro airway models, due to their lack of physiological relevance, are often unable to provide meaningful and accurate toxicological assessments. Advanced in vitro airway models, however, promise to provide more predictive information for use in human airway health. In this report, airway models comprised of fully differentiated primary human bronchial tracheal epithelial cells (HBECs) were generated to assess toxicological response to both short and long-term exposure from either cadmium chloride or pentamidine. Additionally, the toxicological responses from short-term exposure of compounds in airway models were compared to undifferentiated primary HBECS. Here we show that self-constructed airway models may serve as useful tools future airway toxicity research.

ABSTRACT:

Respiratory tract diseases stemming from the inhalation of toxic compounds significantly contributes to the global health burden. Traditional in vitro airway models, due to their lack of physiological relevance, are often unable to provide meaningful and accurate toxicological assessments. Advanced in vitro airway models, however, promise to provide more predictive information for use in human airway health. In these studies, airway models comprised of fully differentiated primary human bronchial tracheal epithelial cells (HBECs) incubated in 24-well plate inserts and cultured under air-liquid interface (ALI) for 4 weeks were generated. The toxicological response to short-term (24 hours) exposure to either cadmium chloride ($CdCl_2$) or pentamidine were evaluated and compared in both airway models and undifferentiated HBECs. In addition, the toxicological response to long-term exposure (1, 2 weeks) to either compound in airway models was also explored. Changes in viability and cytokine expression was quantified and compared in both airway models and undifferentiated HBECs. Additionally, histological imaging (H&E, alcian blue, IHC) was conducted on airway models to visually assess model disruption, inflammation, and tight junction disruption. All airway models expressed dose-dependent response to both $CdCl_2$ and pentamidine exposure, with increased cell death corresponding with increased compound concentrations. Additionally, airway models demonstrated higher resistivity to cell death compared to undifferentiated counterparts. Moreover, exposure to low concentrations resulted in increased cytokine expression relative to untreated controls. Finally, long-term exposure to $CdCl_2$ resulted in model disruption and death, whereas pentamidine exposure demonstrated limited model disruption. These results suggest that airway models may serve as useful tools future airway toxicity research.

INTRODUCTION:

The human respiratory tract is an important subject of study in a variety of fields. Respiratory infections represent the most common form of infection and act as a significant focus in disease research.[1,2] Moreover, inhalation toxicity is the most prominent route of

toxicity exposure, causing an estimated 7 million early deaths worldwide each year according to the World Health Organization.[3,4] In pharmaceutical product development, inhalation serves as a viable of route of therapeutic administration, bypassing the first pass metabolism as well as serving as a more acceptable route of administration for patients relative to intravenous or intradermal delivery.[5-7] Providing relevant models able to recapitulate the human respiratory tract for these diverse scientific fields is of critical importance for global health.

To better serve the needs of human respiratory research, 3-D-airway models have been generated to better emulate the physiological complexity of the bronchial tracheal tract.[8] We seeded primary human bronchial tracheal epithelial cells (HBECs) on microporous membrane supports that were incubated while partially exposed to air, known as air liquid interface (ALI).[9] Following this incubation period, the HBECs fully differentiate to generate airway models containing goblet, ciliated, and basal cell lines, providing a physiologically relevant representation of the bronchial tracheal tract. In contrast, traditional in vitro 2-D-airway models, comprised of undifferentiated primary cells submerged in media, are limited in offering physiologically relevant data.[10] The process of generating airway models, while lengthy compared to traditional models, can be easily performed, providing researchers with an affordable do-it-yourself model.

In the previous work "Evaluating airway ALI model fabrication methods and comparing differentiation potential of primary and hTERT-immortalized epithelial cells," ATCC showcased an optimal method of fabricating airway models comprised of human primary HBECs with consistent full epithelial differentiation using multiple primary cell lots from both ATCC and other commercial vendors. In this report, ATCC investigated the toxicological response from both 3-D airway models comprised of fully differentiated primary HBECs as well as traditional 2-D in vitro models comprised of freshly seeded undifferentiated primary HBECs. Two different primary cell lots were used to generate both models and were subjected to both short and long-term exposure to either cadmium chloride ($CdCl_2$) or pentamidine. Cadmium, a metal utilized in industrial processes, is ranked 7th on the Agency for Toxic Substances and Disease Registry substance priority list as well as categorized as a substance of very high concern by EU's European Chemical Agency due to its toxicity and risk of inhalation exposure.[11,12] In contrast, pentamidine is a potent antimicrobial agent that can be administrated via inhalation and is listed in the World Health Organization list of essential medicines, however adverse side effects from its use are commonly reported.[13,14] Both compounds were chosen to serve as representative substances in the fields of environmental/industrial monitoring and pharmaceutical safety. Here, various concentrations of these two compounds were utilized to compare changes in viability and inflammation from both undifferentiated cells and airway models. These studies reveal not only the differences in exposure response in both models, but also demonstrate the utility in using advanced 3-D airway models as useful tools future airway toxicity research.

MATERIALS AND METHODS:

INITIAL CELL CULTURE

Both lots of primary (ATCC® PCS-300-010™) HBECs were cultured according to ATCC's product sheet recommendations. Briefly, all cells were first grown in ATCC complete airway epithelial growth media, consisting of ATCC Airway Epithelial Cell Basal Medium (ATCC® PCS-300-030™) supplemented with Bronchial Epithelial Cell Growth Kit (ATCC® PCS-300-040™) and 5 mL Penicillin-Streptomycin solution (ATCC® 30-2300™). During culturing and cell proliferation, the cell passage number for all cell lines did not exceed two. Cell growth media was replaced every other day.

For undifferentiated cell models, HBECs were passaged, and collected in growth media at a concentration of 50,000 cells/mL. 96-well plates were prepared, with each well having 0.2 mL of cell solution added (10,000 cells per well). To ensure cell attachment, plates were left at room temperature for at least one hour after seeding, followed by placement in 37°C incubation. The following day, plates underwent toxicity testing. To account for the edge effect, only the interior wells in the 96-well plates underwent testing, with the outer wells filled with 0.2 mL of Dulbecco's Phosphate Buffered Saline (DPBS) (ATCC® 30-2200™).

To fabricate differentiated airway models, permeable trans-well inserts for 24-well plates with PET membrane with 0.4 µm pores (Corning cat# 353095) were placed into Costar clear 24-well multi-well plates (Corning cat# 3524) the day before cell seeding. To prevent edge effects on airway models, inserts were added to interior wells only, with outer wells filled with 2 mL DPBS. The plate inserts were then coated on the apical side with 0.3 mg/mL Collagen solution (Stemcell Technologies cat# 04902) diluted with DPBS, with plates incubating overnight at 4°C.

On the day of seeding, the collagen-coated inserts were apically rinsed twice with 200 µL DPBS, with 0.5 mL of ATCC complete airway epithelial growth media added to the basal side of wells containing trans-well inserts. HBECs were passaged, harvested, and then resuspended in growth media at a concentration of 500,000 cells/mL. The cell solution was added apically to each insert at a volume of 0.2 mL (100,000 cells per well). Following cell seeding, plates were left at room temperature for at least one hour to allow for cell attachment, followed by placement in 37°C incubation. Cells were incubated for 2-3 days until full confluency was reached. If confluency was not reach before 48 hours, both apical and basal side media were replaced with 0.2 and 0.5 mL of complete growth media respectively.

AIRWAY MODEL ALI CULTURING

Once reaching full confluency, both the apical and basal media were removed from each airway model, with the basal media being replaced with 0.5 mL PneumaCult ALI maintenance media (Stemcell Technologies cat# 05001) supplemented with recommended components (Stemcell Technologies cat# 07980 and 07925). In contrast, no replacement media was added to the apical side of the models, partially exposing the cells to the air. Basal media was replaced every other day with fresh complete differentiation media. Cell differentiation was observed visually via microscopy, while weekly images from airway models were collected using an EVOS FL digital microscope (Life Sciences). Following two weeks of ALI incubation, weekly apical washes with (2x) 0.2 mL DPBS were conducted to remove excess mucin from models. To confirm proper airway model formation, TEER measurements were conducted using were collected using an EVOM2 Epithelial voltmeter (World Precision Instruments). After four weeks of ALI incubation and TEER confirmation, models were considered mature and ready for toxicology testing.

UNDIFFERENTIATED CELL TOXICOLOGY TESTING

Following 24 hours after initial cell seeding in 96 well plates, undifferentiated HBECs were subjected to 24-hour exposure to either $CdCl_2$ or pentamidine. Here, 16 different concentrations of $CdCl_2$ (Sigma Aldrich cat# 20298) and pentamidine (USP cat# 1504900) were prepared in DPBS, ranging from 2.5-400 µg/mL (14-2183 µM) or 5.4-2368 µg/mL (9.3-4,000 µM) respectively. Higher pentamidine concentrations required heating solution to 37˚C and vortexing vigorously to ensure complete solubility. Cell media was removed and replaced with 200 µL of respective compound concentration. Blank controls were prepared by administering 0.2mL DPBS to selected cells. Plates were placed in incubator for 24 hours following compound solution administration.

Following 24 hours incubation, 100 µL media was collected to assess IL-8 cytokine expression. Quantification of IL-8 expression was conducted using Human IL-8 ELISA kit (Invitrogen cat# KHC0081) and following the provided instructions. Viability studies were conducted by adding 100 µL CellTiter-Glo 3-D Cell Assay Reagent (Promega cat# G968B) into each sample well. Plates were incubated at room temperature for 30 minutes, followed by pipette mixing and transferring 100 µL of sample into black sided 96-well plates. Samples in wells from the black sided plates were assessed via luminescence using a SpectraMax i3x plate reader (Molecular Devices), with increased relative luminescence units (RLUs) corresponding to increased viability. All RLUs values were corrected by subtracting the media only controls, followed by converting RLU values as percent viability relative to untreated controls [% Viability = 100 × (Sample RLUs/Avg. Untreated RLUs)]. Viability changes in cell models was expressed by calculating the half maximal inhibitory concentration (IC_{50}) using the corrected RLUs values.

FULLY DIFFERENTIATED CELL MODEL TOXICOLOGY TESTING

Following four weeks of ALI, airway models were subjected to 24-hour exposure to either $CdCl_2$ or pentamidine, using the same concentrations administered to undifferentiated HBECs. For 1- and 2-week administration, a reduced number of concentrations were used, focusing on intermediate and lower compound administration. Prior to compound administration, basal media was replaced with fresh 0.5 mL fresh differentiation media, followed by with careful rinsing of the apical side using (2x) 0.2 mL DPBS. To approximate inhalation toxic exposure, 200 µL of respective compound solutions was administered on the apical side of the airway model. For short-term exposure, airway models were incubated 24 hours after administration, followed by sample processing. For both 1- and 2-week exposure, basal media was replaced every 48 hours, with apical media replaced weekly. For sample processing, basal media was removed, followed by 100 µL apical media collection for cytokine expression. Afterwards, 100 µL CellTiter-Glo 3-D Cell Assay Reagent was added to the apical side of the membrane. Following 30 minutes of room temperature incubation, 100 µL of cell solution was transferred to black sided 96-well plates for luminescence measurements.

For histological examination, separate sets of airway models undergoing similar conditions and exposure times were prepared. Following 24 hour, 1- or 2-week exposure time, airway models were fixated and permeabilized using BD cytofix/cytoperm fixation and permeabilization solution (BD cat# BD 554722). Samples were stored in 10% ethanol at 4 ˚C until further processing. Preserved models were paraffin embedded, sectioned, and stained with either H&E or alcian blue, followed by histological examination and imaging. Additional paraffin embedded samples underwent separate ICH staining and imaging using either Rabbit ZO-1 (Fisher Scientific cat# 40-2200) or Rabbit MUC5AC (Cell Signaling Technology Cat# 61193) antibodies.

RESULTS:

HBECs seeded in 24-well plate inserts were incubated under ALI conditions for a period of four weeks to induce epithelial differentiation. During incubation, microscopy images of airway models were taken weekly. Figure 1 illustrates the morphological changes the cells in airway models undertake during ALI, with obvious morphological changes occurring at week 2 (Fig 1C), followed by more pronounced changes occurring at week 3 (Fig 1D). Under these conditions, airway models undergo epithelial differentiation, resulting in mature airway models containing basal, goblet, and ciliated cells. These changes were observed in both primary HBEC lots as well as all airway model

replicates. Moreover, TEER measurements demonstrated acceptable resistivity values and minimal variability between replicates (data not shown).

The first set of viability studies were conducted to assess short-term (24 hour) exposure from $CdCl_2$ on both undifferentiated HBECs and airway models. To visualize potential airway model disruption from $CdCl_2$ exposure, microscopy images of mature airway models were taken 24 hours following compound administration. Figure 2 illustrates the differences in mature airway model responses from DPBS treated (blank controls), low (53.9 µM), or intermediate concentrations (795 µM) of $CdCl_2$. Here, short-term exposure to low concentrations of $CdCl_2$ results in no observable disruption of model integrity relative to DPBS controls, while intermediate exposure to the compound shows widespread cell death, greatly disrupting airway model integrity.

In addition to microscopy imaging, changes in viability were assessed by generating IC_{50} curves from both undifferentiated HBECs and airway models using two different primary HBEC lots (Figure 3). We observed that the undifferentiated airway models demonstrated a gradual and consistent dose-dependent decrease in viability with increased $CdCl_2$ administration (Fig. 3A), with both primary HBEC lots exhibiting IC_{50} values of 87.5 µM ± 10.8 and 92.5 µM ± 10.8 respectively. In contrast, airway models demonstrated higher resistivity to cell death, maintaining nearly 100% viability up to 149 µM $CdCl_2$ exposure. However, the drop in viability in airway models was more pronounced, relative to undifferentiated HBECs (Fig. 3B). The IC_{50} values of airway models lots 1 and 2 were calculated to be 203.1 µM ± 7.2 and 273.7 µM ± 12.3 respectively, a 2-fold increase in IC_{50} values relative to untreated HBECs (Fig. 3C-D).

Viability measurements from short-term pentamidine exposure was also assessed. Figure 4 illustrates both the changes in viability as well as generated IC_{50} curves from both undifferentiated HBECs and airway models following 24-hour pentamidine administration. Similar to results from $CdCl_2$ administration, both lots of undifferentiated primary HBECs demonstrate dose-dependent decrease in viability with increased pentamidine administration, with lots 1 and 2 exhibiting IC_{50} values of 60.4 µM ± 5.5 and 57.1 µM ± 13.5 respectively (Fig. 4A). However, airway models exhibited significantly higher resistance to cell death relative to undifferentiated HBECs, maintaining nearly 100% viability at pentamidine concentrations 1185 µM, as well as maintaining an average viability over 10% even at the highest exposure concentration (Fig. 4B). Here airway model lots 1 and 2 demonstrated IC_{50} values of 2,811 µM ± 201 and 2,279 µM ± 113 respectively, with IC_{50} values averaging over 40-fold higher than undifferentiated primary HBEC counterparts (Fig. 4C-D).

To better visualize changes in airway model structure from short-term $CdCl_2$ exposure, histological analysis on separate sets of exposed airway models was conducted. Figure 5 shows representative images of alcian blue stained airway models incubated in either 0 (DPBS blank controls), 53.9 (low), 147.9 (intermediate), or 2183.4 µM (high) $CdCl_2$ for 24 hours. DPBS blank controls demonstrated appropriate model morphology, showing the presence of goblet and ciliated cells (Fig. 5A). Short-term exposure to low concentrations of $CdCl_2$ resulted no noticeable differences in model morphology (Fig. 5B). In contrast, intermedia $CdCl_2$ exposure clearly results in model deterioration, with decreased model thickness and absence of cells on the membrane support (Fig. 5C). Finally, high levels of $CdCl_2$ exposure resulted in the complete degradation of the airway model, with one or two cells present on the entire membrane (Fig. 5D).

Histological analysis was also conducted on airway models exposed to short-term pentamidine administration. Figure 6 illustrates representative images of alcian blue stained airway models incubated in either 0 (DPBS blank controls), 46.2 (low), 1,185 (intermediate), or 4,000 µM (high) pentamidine for 24 hours. Unlike $CdCl_2$ treated counterparts, airway models demonstrated greater resistance in model degradation from short-term exposure to pentamidine, with both low and intermediate concentrations showing no observable difference in morphology relative to DPBS treated blank controls. However, slight model disruption was only observed in the highest treated (4,000 µM) pentamidine sample (Fig. 6D).

In addition to assessing changes in viability from short-term compound exposure, cytokine expression was also assessed to better examine toxicological response from both compounds. Figure 7 shows the changes in IL-8 expression in both undifferentiated HBECS and airway models from 24-hour exposure from to $CdCl_2$. In both undifferentiated HBECs and airway models, low to intermediate administration of $CdCl_2$ results in increased expression of the proinflammatory cytokine, compared to untreated blank controls. In contrast, models subjected to high $CdCl_2$ administration exhibited cytokine expression levels similar to or lower than blank controls, which was attributed to cell death. In the pentamidine administered samples, high pentamidine administration resulted in little to no detectable IL-8 in both airway models and undifferentiated HBECs, whereas samples administered with low pentamidine concentrations showed lowered cytokine expression relative to blank controls (data not shown).

Following the conclusion of the short-term viability studies, airway models were subjected to one- or two-week exposure to either $CdCl_2$ or pentamidine. Figure 8 displays the changes in viability and cytokine expression from continuous exposure to either compound. After 1-week of $CdCl_2$ exposure, both airway model lots exhibited slightly elevated viability measurements from low exposure concentrations relative to untreated controls, probably as a function of wound healing response. In contrast, moderate long-term $CdCl_2$ administration resulted in significant decrease in airway model viability. Additionally, 2-week exposure results exhibited similar trends, with low $CdCl_2$ concentrations demonstrating near equivalent viability response relative to untreated controls (Fig. 8A). Viability measurements taken

from long-term pentamidine administration resulted in similar trends to $CdCl_2$ exposure, with low pentamidine concentrations demonstrating comparable viability response to blank controls whereas long-term moderate pentamidine exposure resulted in decrease viability (Fig. 8B). Cytokine expression was also assessed using apical washes collected at the end of compound administration (Fig. 9C). Similar to short-term testing, airway models demonstrated elevated levels of cytokine expression to low cadmium administration following 1 week incubation relative to untreated controls, whereas moderate cadmium administration results in low cytokine expression, attributed to cell death. There was no observable trend between increased cytokine expression to increased compound administration following 2-week administration, which was attributed to suboptimal cytokine sample collection from long-term studies (data not shown).

Parallel with long-term viability measurements, histological assessments were also conducted on separate airway model samples. Figure 9 shows representative images of alcian blue stained airway models treated with either low to moderate administrations of either $CdCl_2$ or pentamidine for one week. Increasing $CdCl_2$ administration during this period results in progressively deteriorating airway model integrity. Pentamidine exposure showed a similar, albeit a more gradual trend, with model integrity being better preserved from long-term pentamidine exposure. These trends were observed in two week administered samples as well (data not shown).

Finally, separate IHC staining and imaging was conducted to visualize potential ZO-1 protein disruption from long-term $CdCl_2$ exposure as well as increased MUC5AC expression short-term pentamidine administration (Figure 10). Representative IHC-stained images of airway models stained for ZO-1 protein demonstrated that decreased ZO-1 expression is correlated to increased $CdCl_2$ administration, relative to blank controls (Fig. 10A-C). In contrast, no observable correlation was found between with increased MUC5AC expression from increasing pentamidine administration (Fig. 10D-F). This result was attributed to the preparation of histology samples, which may have resulted in the washing and removal any excess mucin from the airway model samples.

DISCUSSION:

In these studies, self-constructed airway models comprised of fully differentiated HBECs were fabricated for use in toxicological studies. Here, the toxicological response between airway models and freshly seeded undifferentiated HBECs from short-term administration of two different compounds were compared. Moreover, this study also examined the variation between models comprised of two separate primary cell production lots. Finally, long-term exposure studies of airway models were also explored.

During these studies, compounds were administered to the apical side of airway models to better approximate the physiologically relevant exposure of the human lung to toxic compounds. We observed that airway models subjected to short-term $CdCl_2$ or pentamidine exposure exhibited average IC_{50} values of 238 and 2545 µM respectively. To our knowledge, no relevant study has yet been conducted to assess changes in viability in airway models from 24-hour exposure to pentamidine. In contrast, a previous study testing airway models to short-term $CdCl_2$ exposure estimated IC_{50} to be within a range 100-300 µM, in agreement to our findings.[15] However, the referenced study administered $CdCl_2$ on the basal side. This difference may not affect airway models comprised of only HBECs; however, co-culture models may not respond in a physiologically relevant manner to compound administration through basal media.

Short-term cytokine results aligned with our expectations, with low-moderate $CdCl_2$ administration results in higher cytokine expression relative to blank controls, whereas high compound fails to elicit higher cytokine expression due to greater cell death. In contrast, pentamidine administration failed to induce increased cytokine expression. Previous in vitro studies showed that pentamidine exposure inhibits IL-8 expression, which was observed in this study as well.[16] During long-term testing no trend was observed during 2-week incubation, which was attributed to cytokine sample loss when basal media was replaced during the study. Although basal media replacement is vital in sustaining airway model viability, any media or solution incubated with airway models should be collected and assessed during the study. Long-term viability measurements were unaffected to this incident due to directly assessing primary cell metabolism.

These studies showcase how self-fabricated airway models can be utilized to provide data that's more physiologically relevant to the human airway model. This was clearly demonstrated when comparing the response from both undifferentiated HBECs and airway models from pentamidine administration. Moreover, the seeding of additional cells, such as fibroblasts, dendritic, or endothelial cells are possible using this airway model fabrication method and may offer additional insights utility in toxicology studies.

ACKNOWLEDGEMENTS:

Histological processing and imaging were conducted by VitroVivo Biotech LLC.

FIGURES AND TABLES:

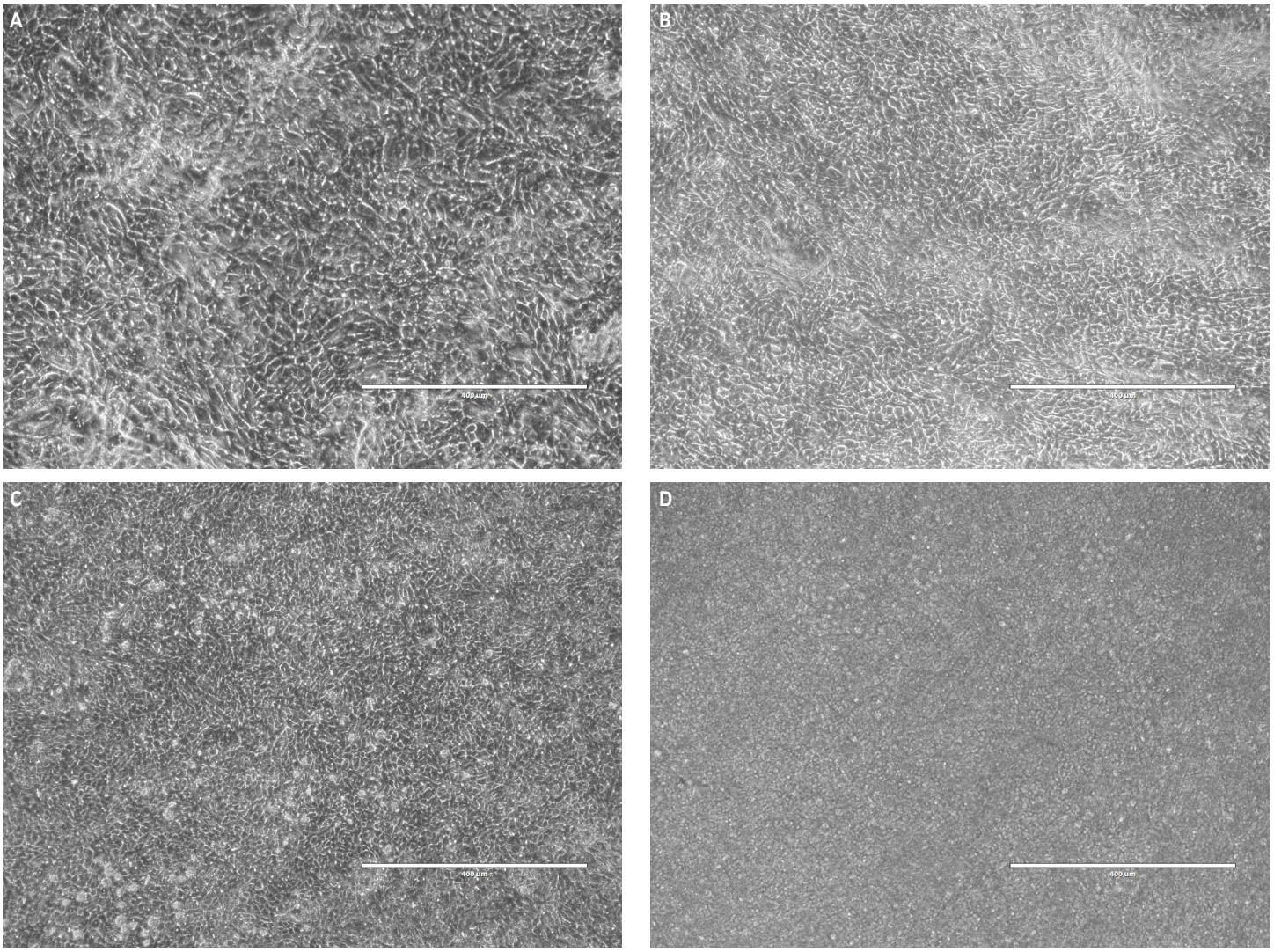

Figure 1: Representative microscopy images of primary bronchial epithelial cells under (A) 0, (B) 1, (C) 2 and (D) 3 weeks of ALI. Prolonged incubation under ALI conditions induces fully epithelial differentiation in airway models. Scale bars represent 400 µm.

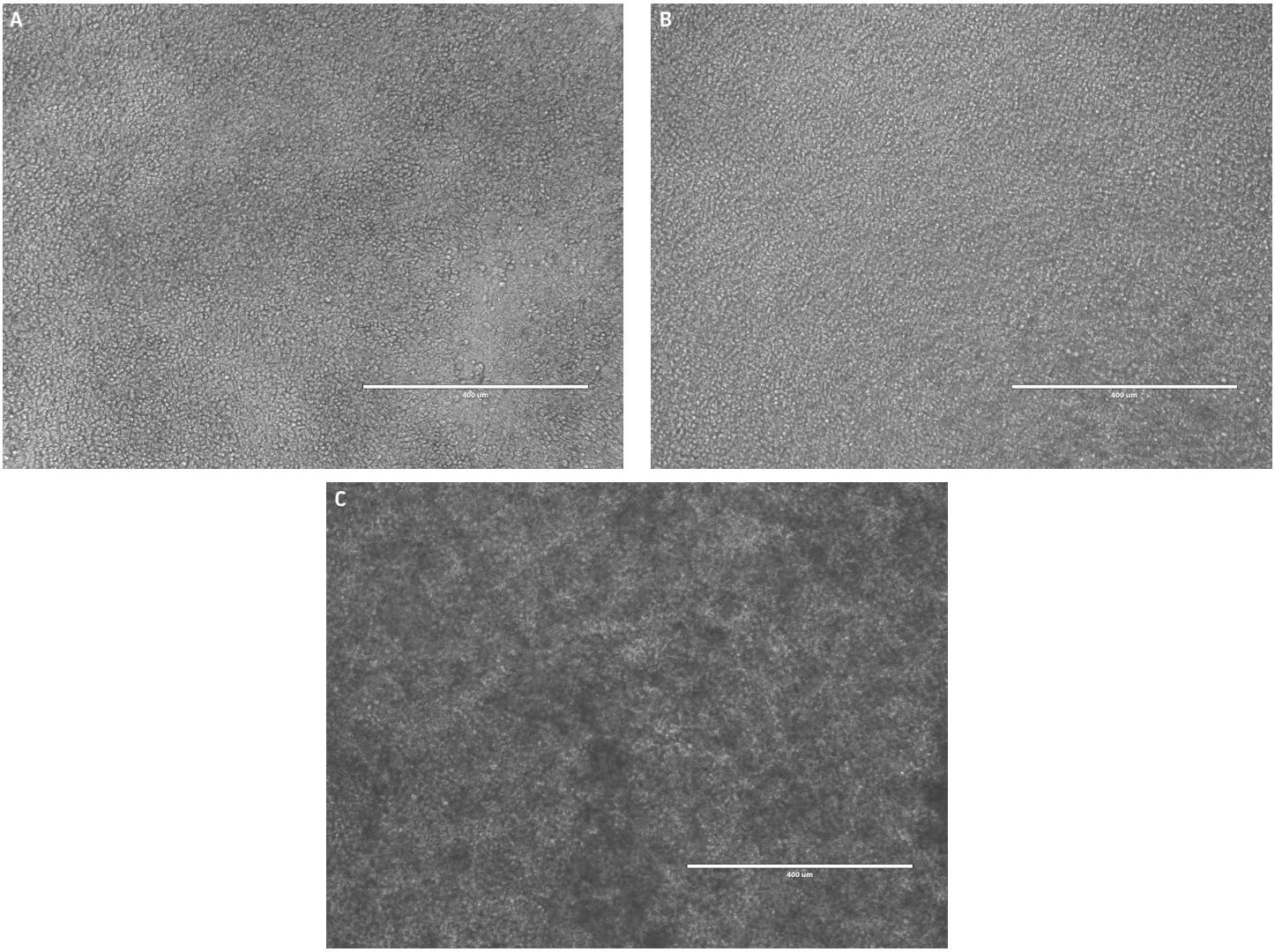

Figure 2: Representative microscopy images of airway models apically treated with either (A) 0, (B) 53.9 or (C) 795.6 µM $CdCl_2$ for 24 Hr. No observable differences were seen between airway model blank controls and models administrated with low concentrations of $CdCl_2$. In contrast, intermediate $CdCl_2$ exposure results in high levels of cell death and model disruption (floating black spots). Scale bars represent 400 µm.

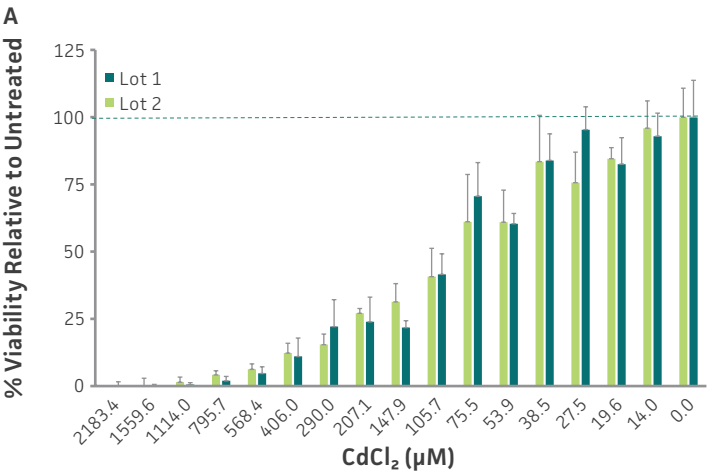

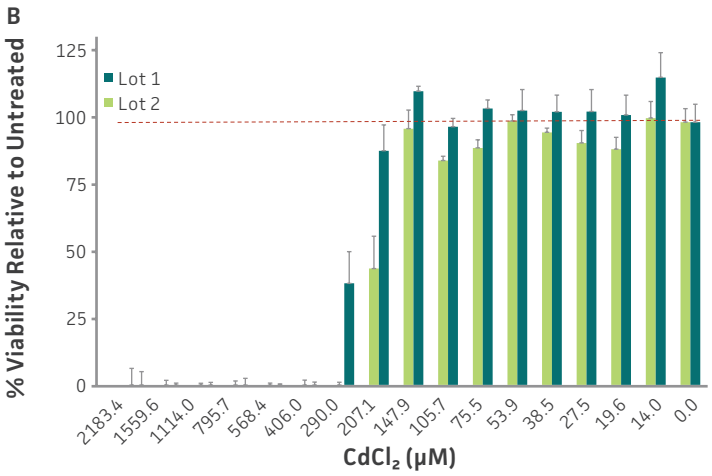

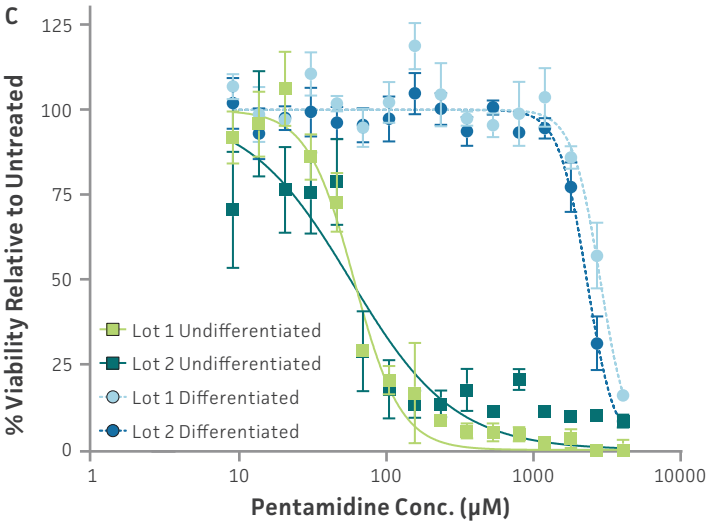

D

Cadmium Chloride IC_{50} values (µM)	
Sample Name	**IC_{50} Value (µM)**
Undifferentiated Lot 1	87.47 ± 10.8
Undifferentiated Lot 2	92.49 ± 10.8
Differentiated Lot 1	203.1 ± 7.2
Differentiated Lot 2	273.7 ± 12.3

Figure 3: Changes in viability between (A) undifferentiated HBECs and (B) airway models from 24-hour exposure to $CdCl_2$. Both undifferentiated HBECs and differentiated airway models were assessed by generating (C) IC_{50} curves and (D) comparing IC_{50} values between the two groups. Airway models demonstrated higher resistivity to cell death and IC_{50} values, relative to undifferentiated HBECs.

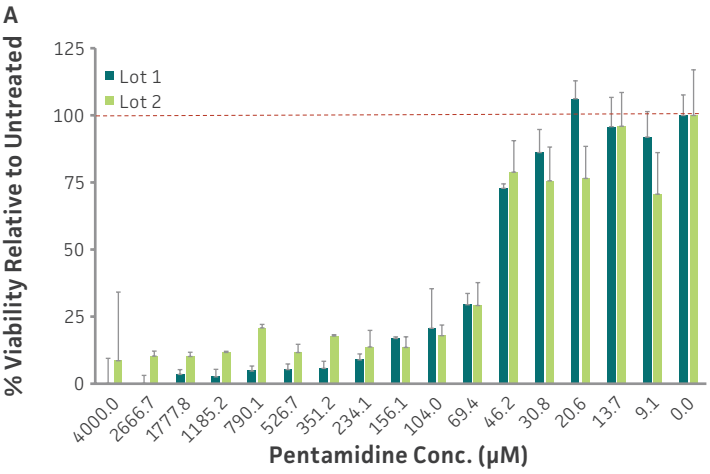

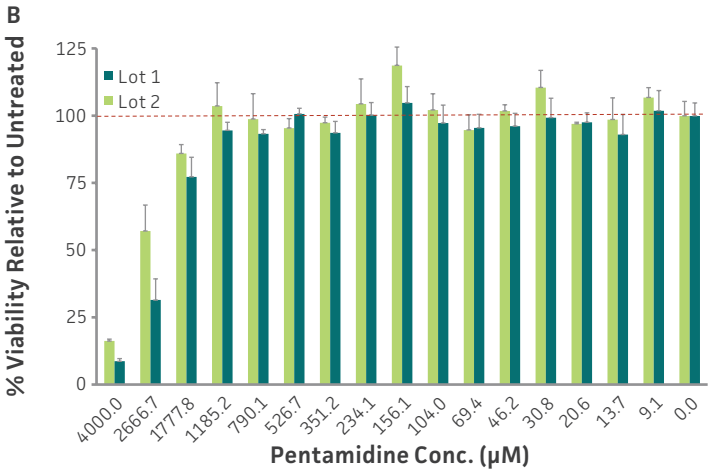

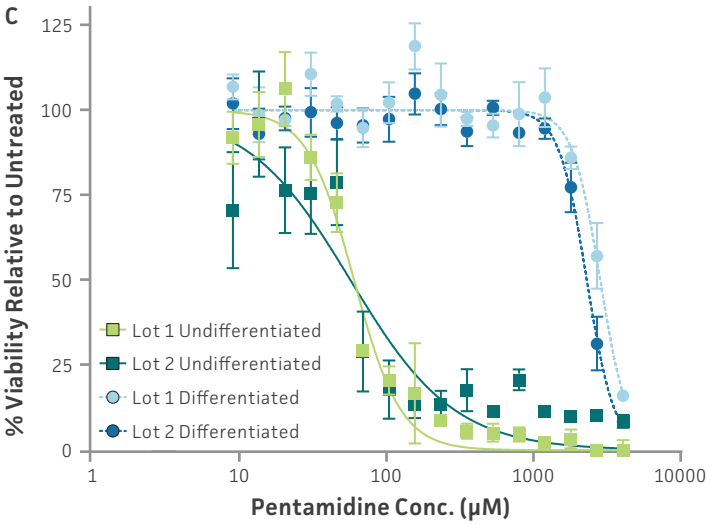

D

Pentamidine IC_{50} values (µM)	
Sample Name	**IC_{50} Value (µM)**
Undifferentiated Lot 1	60.4 ± 5.5
Undifferentiated Lot 2	57.1 ± 13.5
Differentiated Lot 1	2811 ± 200.5
Differentiated Lot 2	2279 ± 113

Figure 4: Changes in viability between (A) undifferentiated HBECs and (B) airway models from 24-hour exposure to pentamidine. Both undifferentiated HBECs and differentiated airway models were assessed by generating (C) IC_{50} curves and (D) comparing IC_{50} values between the two groups. Airway models demonstrated significantly higher resistance to cell death and as well as over 40-fold higher IC_{50} values, relative to undifferentiated HBECs.

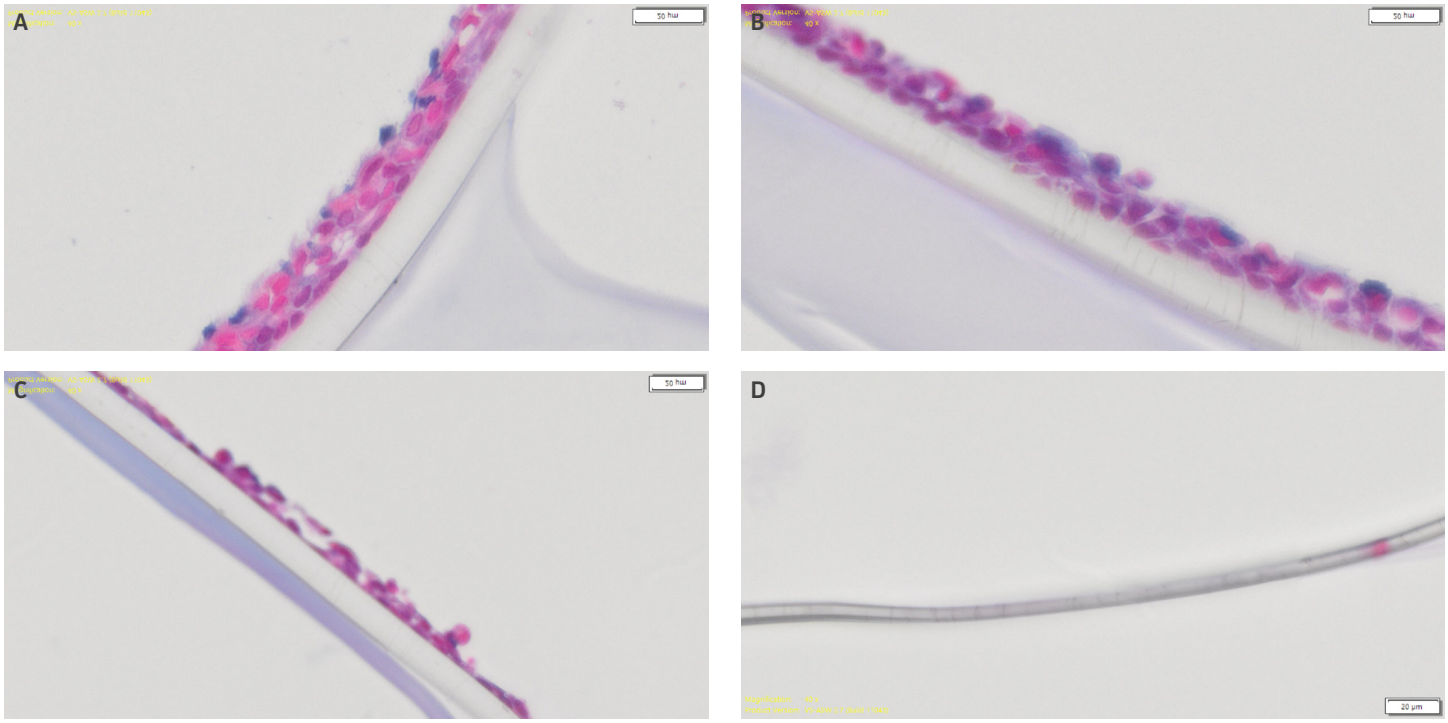

Figure 5: Representative alcian blue stained images of airway models apically treated with 24-hour exposure to either (A) DPBS blank controls, (B) 53.9, (C) 147.9, or (D) 2183.4 µM $CdCl_2$. Increased $CdCl_2$ administration results in greater airway model disruption and cell death. Scale bars represent 20 µm.

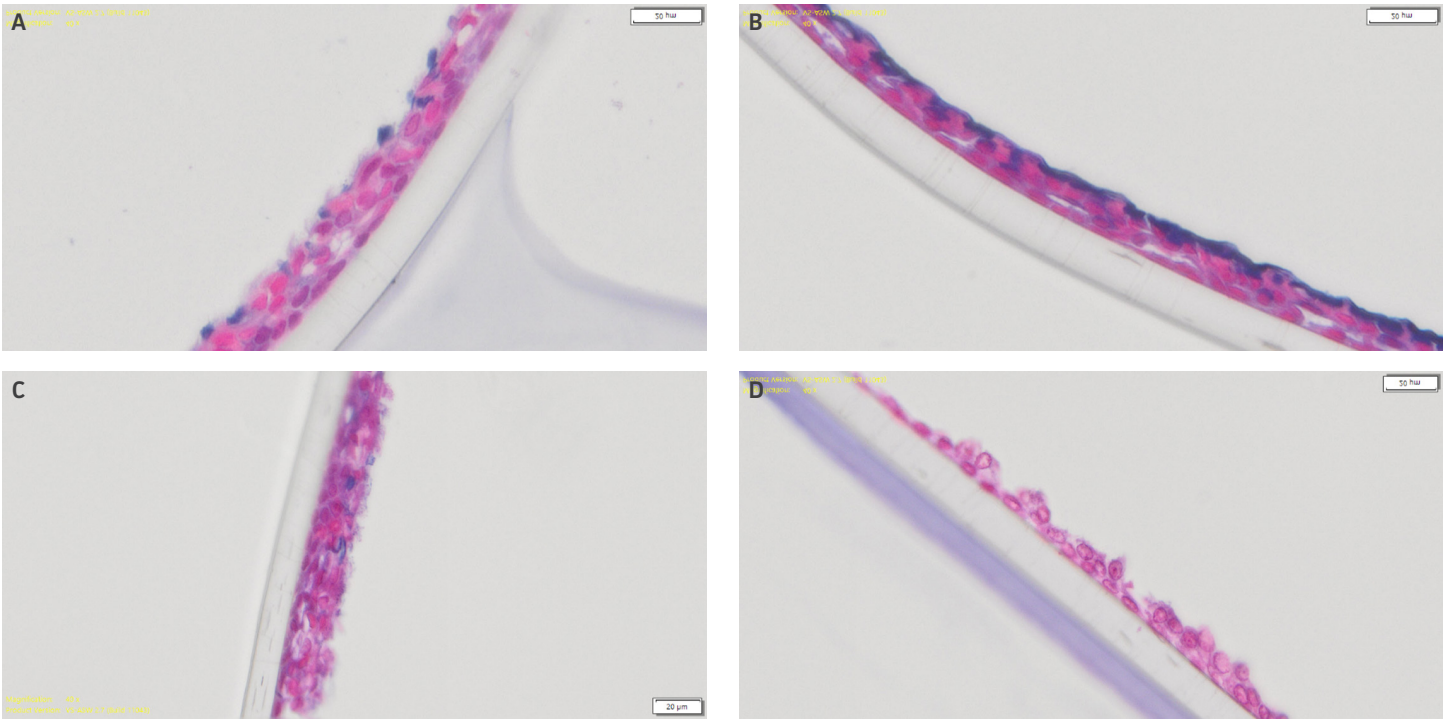

Figure 6: Representative alcian blue stained images of airway models apically treated with either (A) DPBS blank controls, (B) 46.2, (C) 1,185, or (D) 4,000 µM pentamidine for 24 Hr. Compared to $CdCl_2$ counterparts, airway models demonstrated no observable model degradation from short-term pentamidine exposure, except for the highest administered dosage of 4,000 µM, which exhibited moderate model disintegration. Scale bars represent 20 µm.

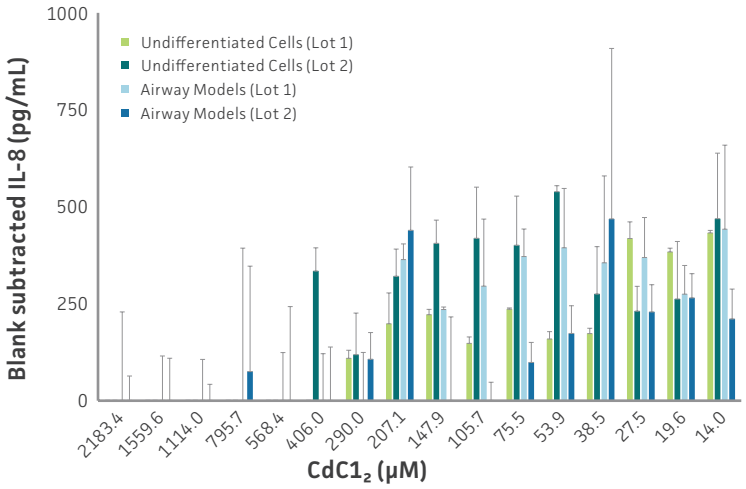

Figure 7: Analysis of IL-8 cytokine expression from 24-hour administration of $CdCl_2$ to both undifferentiated HBECs and mature airway models. Values are shown as blank subtracted. Low concentrations of $CdCl_2$ results in increased proinflammatory cytokine expression, relative to blank controls. In contrast, intermediate to high administration, results in decreased expression, due to cell death.

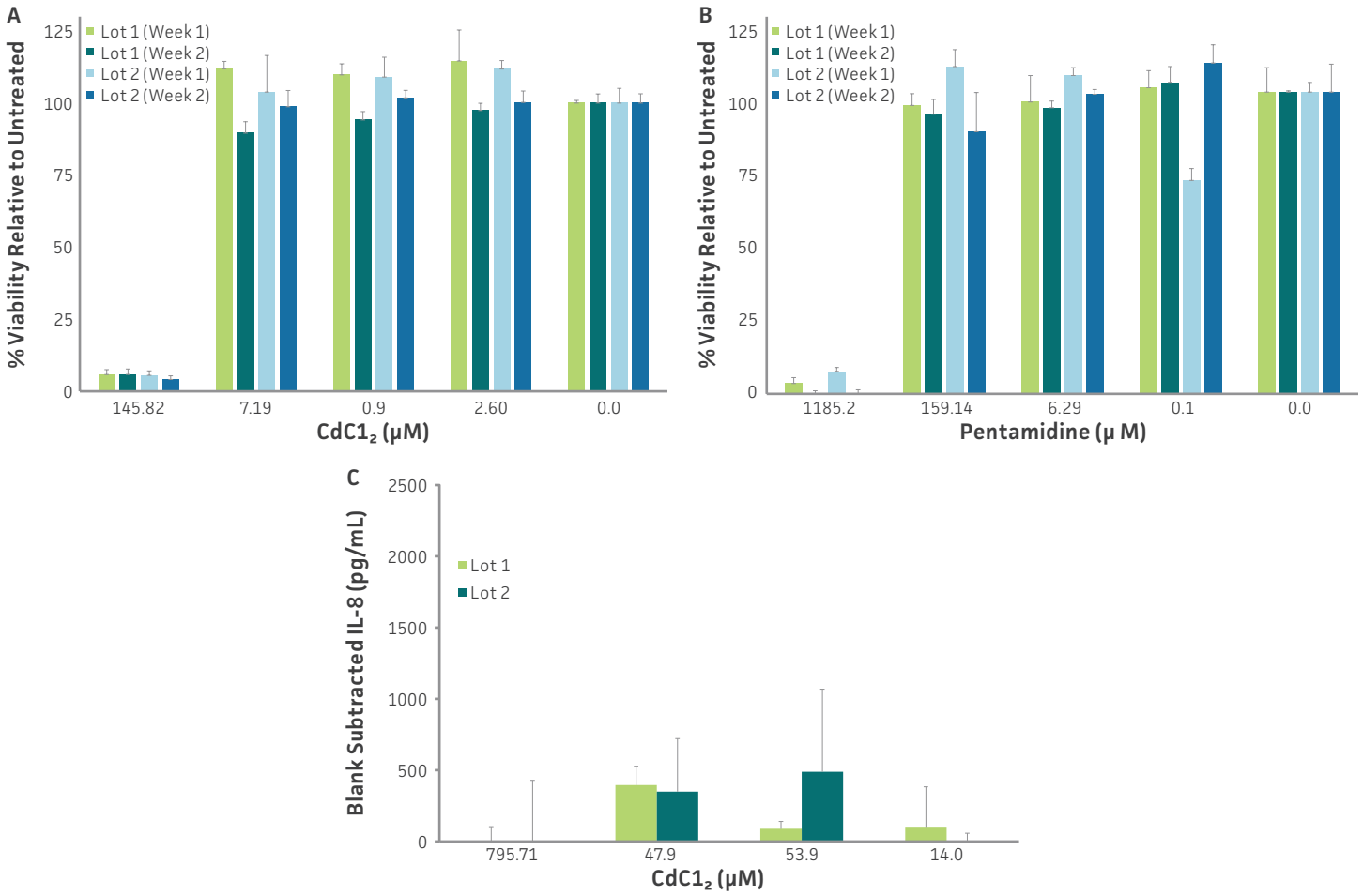

Figure 8: **Changes in viability in airway models exposed to either (A) $CdCl_2$ or (B) pentamidine for 1 and 2 weeks, (C) as well as cytokine expression following 1 week administration of $CdCl_2$.**

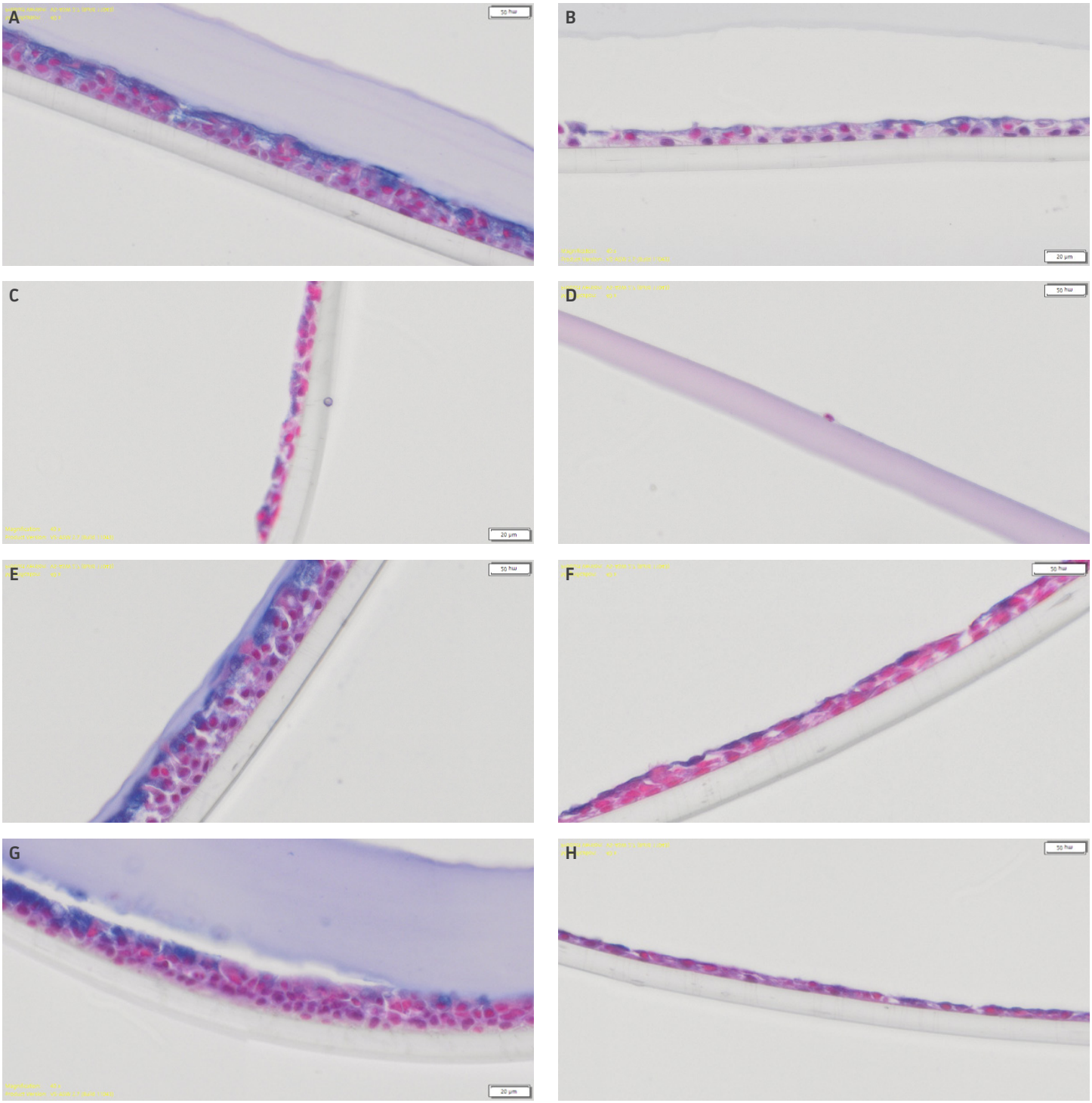

Figure 9: Representative alcian blue stained images of airway models apically treated with either (A) 0, (B) 14.0, (C) 53.9, or (D) 795.6 µM $CdCl_2$, or (E) 0, (F) 46.2, (G) 156, (H) 1185 µM pentamidine for 1 week. Long-term exposure from low or moderate concentrations of $CdCl_2$ results in airway model disruption. In contrast, airway model integrity is better preserved from long-term pentamidine exposure. Scale bars represent 20 µm.

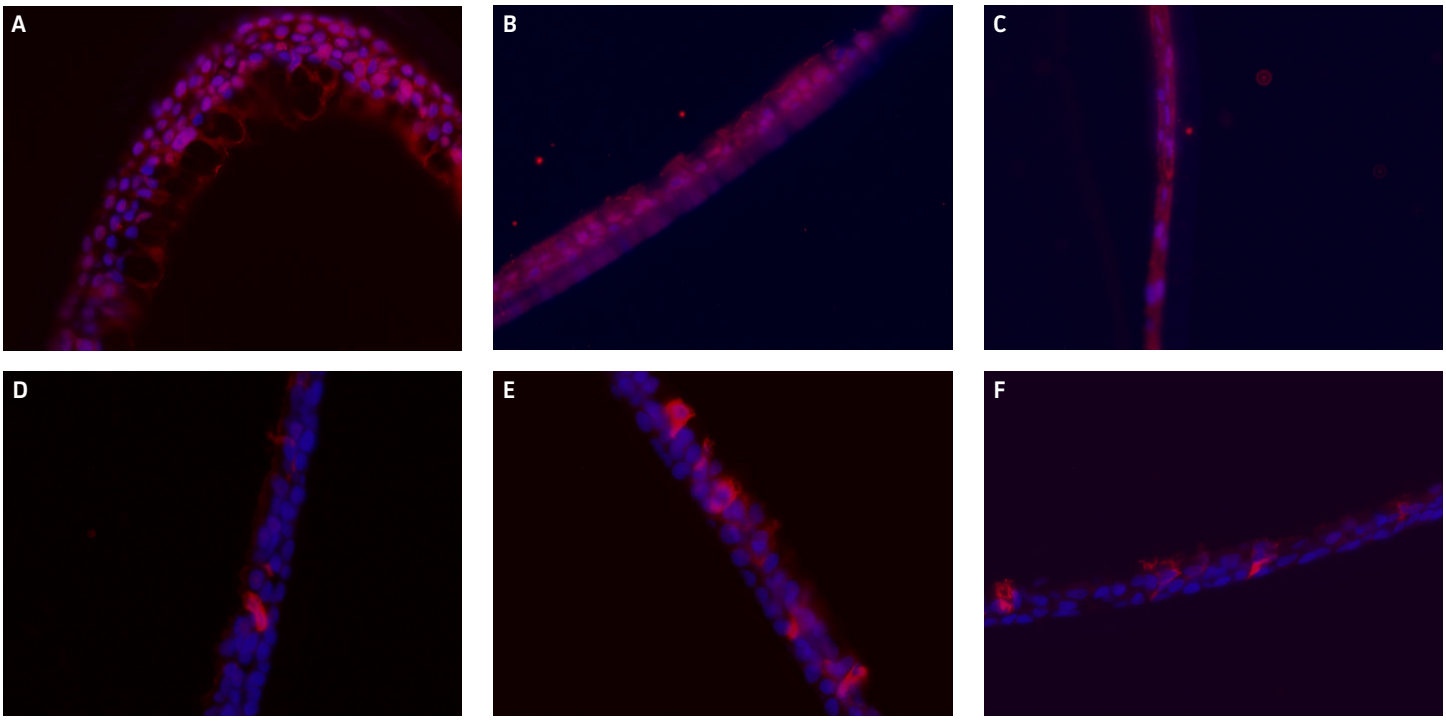

Figure 10: Representative ICH-stained images of (A) untreated control airway models, airway models exposed to (B) 14.0, or (C) 147.9 μM $CdCl_2$ for 2 weeks. ZO-1 protein expression is shown as red with DAPI control in blue. ZO-1 protein disruption is associated with increased $CdCl_2$ exposure. Representative ICH-stained images of airway models treated with (D) 0, (E) 9.1, (F) 46 μM pentamidine for 24 Hr. MUC5AC expression shown as red with DAPI control in blue. There was no correlation with increased MUC5AC expression with increasing pentamidine administration.

BACK TO CONTENTS

REFERENCES:

1. *Estimates of the global, regional, and national morbidity, mortality, and aetiologies of lower respiratory infections in 195 countries, 1990-2016: a systematic analysis for the Global Burden of Disease Study 2016*. Lancet Infect Dis, 2018. **18**(11): p. 1191-1210.
2. Wang, X., et al., *Global burden of acute lower respiratory infection associated with human metapneumovirus in children under 5 years in 2018: a systematic review and modelling study*. Lancet Glob Health, 2021. **9**(1): p. e33-e43.
3. Burnett, R., et al., *Global estimates of mortality associated with long-term exposure to outdoor fine particulate matter*. 2018. **115**(38): p. 9592-9597.
4. Organization, W.H. *9 out of 10 people worldwide breathe polluted air, but more countries are taking action*. 2018; Available from: https://www.who.int/news/item/02-05-2018-9-out-of-10-people-worldwide-breathe-polluted-air-but-more-countries-are-taking-action.
5. van den Berg, A.A., et al., *Intravenous or Inhaled Induction of Anesthesia in Adults? An Audit of Preoperative Patient Preferences*. 2005. **100**(5): p. 1422-1424.
6. Stewart, K.D., et al., *Preference for pharmaceutical formulation and treatment process attributes*. Patient Prefer Adherence, 2016. **10**: p. 1385-99.
7. Losi, S., et al., *The role of patient preferences in adherence to treatment in chronic disease: a narrative review*. Drug Target Insights, 2021. **15**: p. 13-20.
8. Cao, X., et al., *Invited review: human air-liquid-interface organotypic airway tissue models derived from primary tracheobronchial epithelial cells-overview and perspectives*. In Vitro Cell Dev Biol Anim, 2021. **57**(2): p. 104-132.
9. Rayner, R.E., et al., *Optimization of Normal Human Bronchial Epithelial (NHBE) Cell 3-D Cultures for in vitro Lung Model Studies*. Sci Rep, 2019. **9**(1): p. 500.
10. Bérubé, K., et al., *Human primary bronchial lung cell constructs: the new respiratory models*. Toxicology, 2010. **278**(3): p. 311-8.
11. Faroon, O., et al., *Toxicological Profile for Cadmium*. 2012, Agency for Toxic Substances and Disease Registry (US), Atlanta (GA).
12. Nordberg, G.F., et al., Risk assessment of effects of cadmium on human health (IUPAC Technical Report). 2018. **90**(4): p. 755-808.
13. Scheld, M.W., B. Wispelwey, and R.D. Pearson, *Pentamidine: A Review*. Infection Control & Hospital Epidemiology, 1991. **12**(6): p. 375-382.
14. Monk, J.P. and P. Benfield, *Inhaled Pentamidine*. Drugs, 1990. **39**(5): p. 741-756.
15. Cao, X., et al., *Tight junction disruption by cadmium in an in vitro human airway tissue model*. Respir Res, 2015. **16**(1): p. 30.
16. Van Wauwe, J., et al., *The inhibitory effect of pentamidine on the production of chemotactic cytokines by in vitro stimulated human blood cells*. Inflamm Res, 1996. **45**(7): p. 357-63.

10801 University Boulevard
Manassas, Virginia 20110-2209

703.365.2700 703.365.2701 sales@atcc.org www.atcc.org

AP-012023-v01

Further reading and resources

1. Toxicology: Models for Every Stage of Your Toxicity Screening Studies
2. Modeling, Screening, Characterizing
3. Pharmacology, Exploratory, Toxicology
4. Preclinical Toxicology PK Metabolism
5. Primary Cells: Essential Tools to Advance Your Life Science Research and Drug Discovery
6. Immune Cells: Human Primary Immune Cells for Immunotherapy Research
7. hTERT-immortalized Cells: A Breakthrough in Cell Biology Research
8. Human Cells: ATCC Human Cells are Invaluable for your Public Health Research
9. Establishment of 3-D Neurosphere Culture from Human iPSC-Derived Neural Progenitor Cells
10. Evaluating Airway ALI Model Fabrication Methods
11. ATCC Human Bronchial/Tracheal Epithelial Cells: Improving Functional Studies
12. Comprehensive Gene Expression Analysis and Neurotoxicity Testing of Human iPSC-derived Neural Progenitor Cells and Neurons
13. hTERT-immortalized and Primary Keratinocytes Differentiate into Epidermal Structures in 3-D Organotypic Culture
14. ATCC's Toxicology Portfolio: Tools for Every Stage of Your Preclinical Drug Development Workstream Webinar
15. Toxicology portfolio of products